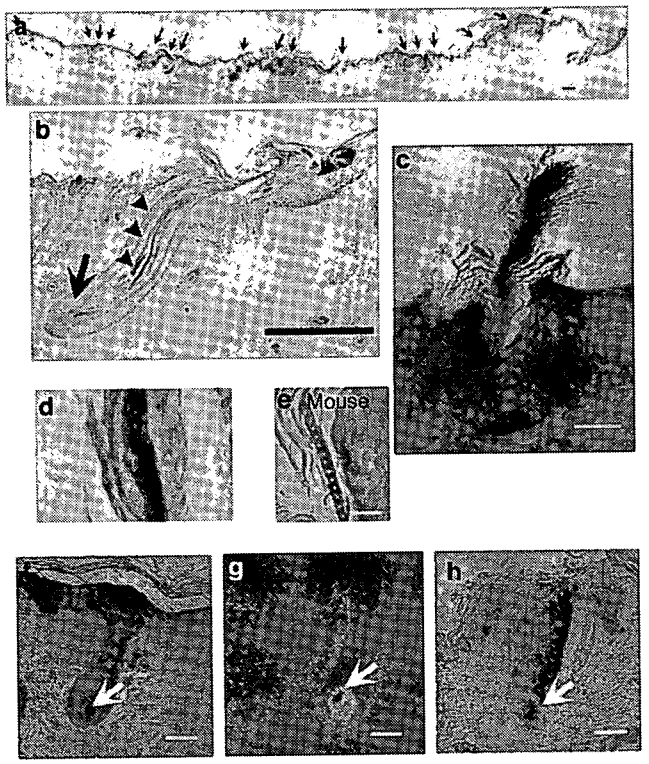

Figure 3. Human-murine chimeric hair follicle-like structures are generated on the dorsal skin of nude mice (human neonatal keratinocytes/murine DPE). Hair follicle-like structures were formed by cellular co-grafting of human neonatal foreskin-derived keratinocytes and murine DPE in 4 weeks. (**a**) A whole section of the graft: arrows indicate the hair follicle-like structures. (**b**) Each follicle formed a few layers of the epithelial cells (arrowheads) and the innermost region was clearly keratinized, which appears to correspond to human hair cortex and medulla. Arrow indicates presumable DP. (**c**) Occasionally, a hair-shaft like fiber was observed inside a follicle, which even emerged from the skin surface. (**d**) The shaft had pigmented melanin deposition in the inner layers. (**e**) For comparison, a normal murine hair is shown, that has characteristic banded medulla. Note that the hair follicle-like structure formed is larger compared to the murine follicle (**d** *vs* **e**). These hair follicle-like structures were often associated with condensed dermal cells (arrows in (**b**, **f–h**)). (**f**) HE staining of adjacent section of (**g**) and (**h**). (**g**) Hoechst 33258 nuclear staining showed that the follicular epithelium originated from human cells (uniform nuclear staining), whereas the cells of mouse origin reside at the bottom (brighter multinuclear staining, indicated by an arrow). (**h**) DNA *in situ* hybridization for *Alu*I-repeated sequence distinctive of human species also proved that the epithelium was of human origin. Bar (**a**, **b**) = 200 μm, (**c**) = 100 μm, (**d**, **e**) = 25 μm, (**f–g**) = 50 μm.

of the chimeric hair follicle-like structures (Figure 4a). The hair keratin-specific antibody, AE13, gave a faint but specific signal at the innermost regions of the formed hair follicle-like structures (Figure 4b). In the epithelium of the structures, strong signals for both S100A8 and S100A9 mRNA were observed (Figure 4c and d). The boundary between the structures and the surrounding epidermis is not as clear as in mature hair follicles, but signals for Hb1, S100A8, and S100A9 mRNAs were absent in the interfollicular epidermis (insets of Figure 4a, c and d, showing lower magnification). Alkaline phosphatase activity was detected in the globular area located at the bottom of the structures (Figure 4e), which indicates the nature of the DP.

Contrary to the above results, neither keratin 15 (hair stem-specific keratin expressed in the bulge) nor transglutaminase 1 (a terminal differentiation marker of follicles and epidermis) was stained in the chimeric hair follicle-like structures (Figure 4f and g). Associated condensed mesenchymal cells (presumably DP cells) were also negative for versican (Figure 4h), which is an active (anagen) DP marker during late development and hair cycle stage.

To further characterize the chimeric hair follicle-like structures, we examined if they express markers reported to be expressed during hair development. The signal for Ki67 was detected at the outermost layer of the hair follicle-like structure (Figure 5a). CD44 was also stained clearly at the cell periphery of outer cell layers (Figure 5b). Msx-2 was observed at the inner side of the follicular epithelium (Figure 5c). The signal for p63 was detected in cells at the outer layer (Figure 5d). These molecular characteristics of the hair follicle-like structures are summarized in Table 2.

Adult epidermal cells are also capable of generating hair follicle-like structures

To examine if adult epidermal cells also possess the differentiation ability, they were co-grafted with murine DPE (Figure 6a and c). Hoechst staining revealed that rat keratinocytes exist in the epidermis and some are occasionally incorporated within the epithelia of the hair follicle-like structures (Figure 6b and d). Further, co-grafts of adult human foreskin-derived epidermal cells (1×10^7 cells) with murine DPE demonstrated that human adult cells also have the same ability to differentiate into follicular keratinocytes as neonatal foreskin-derived epidermal cells (Figure 6e and f).

Passaged keratinocytes lose their differentiation potential

In addition to primary cultures of human neonatal foreskin-derived keratinocytes, those passaged in culture (1×10^6–1×10^7 cells per graft) were subjected to co-grafting with murine DPE. As shown in Table 1, neonatal keratinocytes after the first passage still generate chimeric human hair follicle-like structures as with primary cultures, although the efficiency was reduced. However, in later passages, these foreskin-derived keratinocytes lost their potential to differentiate into the follicular epithelium, as any hair follicle-like structures were not found in the entire graft. Adult epidermal cells also lost their differentiation potential after the second passage, similar to neonatal ones.

DISCUSSION

Using a cell-based grafting procedure, our study demonstrates that human glabrous foreskin-derived epidermal cells possess the potential to differentiate into follicular epithelium. The incorporation of human epidermal cells into rodent hair has been previously shown by grafting on immunodeficient mice of intact skin tissue or epidermal sheets combined with non-human dermal sheets before grafting (Ferraris *et al.*, 1997, 2000). However, this is the first report to demonstrate

Table 1. Generation of human/mouse chimeric hair follicle-like structures and the conditions of the grafted human keratinocytes

Cell condition	Follicle-like structure generation[1]	Density[2] (isolated[3])	Cluster density[4] (structures in a cluster[5])
Neonatal			
Primary (P0)	4/4	13.3±9.5 (2.7±1.3)	3.5±3.3 (3.3±1.3)
P1	4/9	2.3±2.2 (1.3±1.9)	0.2±0.3 (0.3±0.3)
P2	0/2		
P3	0/3		Not estimated
P4	0/2		
Adult			
Intact	1/1		
Primary (P0)	1/1		Not estimated
P1	1/4		
P2	0/3		

Various passages of foreskin-derived human keratinocytes were co-grafted with murine DP-enriched dermal component (DPE) on the dorsal skin of nude mice. Generation of human/murine chimeric hair follicle-like structures was assessed in 3–4 weeks.
[1]Number of recipient(s) in which the chimeric hair follicle-like structures were generated/total number of recipient(s).
[2]As for recipients in which the chimeric hair follicle-like structures were generated, the number of structures in three non-overlapping sections (corresponding to approximately 3 cm length) were estimated. The mean values±standard deviation (SD) of four recipients are listed.
[3]The density of the "isolated" (as defined in the Materials and Methods section) chimeric hair follicle-like structures are indicated as in parenthesis (mean values±SD of four recipients).
[4]The "cluster" (as defined in Materials and Methods) density of chimeric hair follicle-like structures are indicated as mean values±SD of four recipients.
[5]The number of chimeric hair follicle-like structures within a cluster is shown as mean values±SD of four recipients.

consistent generation of hair follicle-like structures consisting of human cells from cell suspensions, and to characterize them by molecular marker expression.

A key factor for generation of these hair follicle-like structures is possibly the use of murine DP cells as the mesenchymal component, which is the same species as the recipient. As has been reported by Ferraris *et al.* (1997), human epidermal cells are easily replaced by host mouse keratinocytes after grafting on nude mice. Our initial xenografting experiments using mouse and rat combinations revealed that the hair reconstitution was apparently less efficient when rat dermal cells were used (Figure S1c). The use of lower passages and larger numbers of keratinocytes (5×10^6–1×10^7 cells/graft) than the previous report (Ferraris *et al.*, 1997) may have also affected the results. Differences in culture conditions may be another factor: the serum-free monolayer culture method was used in this study and the 3T3 feeder layer method (Rheinwald and Green, 1975) was used by Ferraris *et al.* (1997). However, recent observations revealed that keratinocytes cultured in the latter conditions also generated follicle-like structures (Kishimoto *et al.*, unpublished data), thus this possibility may be excluded.

Further, the use of neonatal (days 1–3) DPE, rather than the use of embryonic dermal cells which may contain pluripotent dermal cells or cells of epidermal origin, clarified the contribution of the committed DP cells in the dermis. Although complete exclusion of epidermal cells from the dermal cell fraction prepared by the freeze-thawing process is unlikely (Tse and Cooper, 1990), FACS analysis of freeze-thawed dermal cells from versican transgenic mice shows that DP cells survived selectively compared to CD49f-positive cells. CD49f is the α6-integrin surface marker and represents basal keratinocytes, including epidermal stem cells (Li *et al.*, 1998) and the follicular epithelium (Ghali *et al.*, 2004), but not suprabasal keratinocytes. Possible contaminating suprabasal keratinocytes, however, would not contribute to hair formation, because no hair follicle-like structure was formed by the DPE alone. Besides, keratinocytes in the chimeric hair follicle-like structures were determined to be human, and were not contaminating murine epidermal cells.

In these transgenic mice, GFP-positive cells are expressed in the upper dermis region where dermal fibroblasts contact epidermal keratinocytes, based on the observation by the formalin-fixed tissue (Shimizu and Morgan, 2004). Although the majority of GFP fluorescence we observed in partially digested and relatively intact neonatal transgenic mouse skin was from DP (Figure 1a and b), cells in the upper dermis may also exert DP-like activity in terms of hair inductivity (Shimizu and Morgan, 2004).

Our study also emphasizes the importance of the dermal cell fraction as compared to the epidermal fraction on a cell number basis. This may imply that neonatal epidermal cells include a substantial number of undifferentiated stem-like cells or that they aggregate easily. The need for a large number of DPE cells may reflect the substantial existence of a sub-population of non-DP dermal cells with a low inductive property. In a murine hair follicle reconstitution system by intradermal injection of epithelial and mesenchymal cells, it is estimated that 5,000 dermal cells and 2,500 epidermal cells produce a single follicle (Zheng *et al.*, 2005). Therefore, in our system, which uses 10 million cells per graft, only a few percent of cells are supposed to contribute to generate a follicle-like structure. It is not clear whether this is mainly because of possible encounters between epithelial aggregates and DP cells and/or to a low percentage of "stem cell"-like undifferentiated epidermal cells.

Together with a previous report (Ferraris *et al.*, 1997), our study clearly demonstrates that epidermal cells which are originally isolated from glabrous regions of the skin possess the potential to differentiate into follicular epidermis. We also show that this phenomenon is observed with adult human epidermis. Regarding mesenchymal cell components needed for hair formation, a recent report indicated that dental papilla cells also possess hair follicle-forming ability (Reynolds and Jahoda, 2004). This indicates that under certain circumstances, both epithelial and mesenchymal compo-

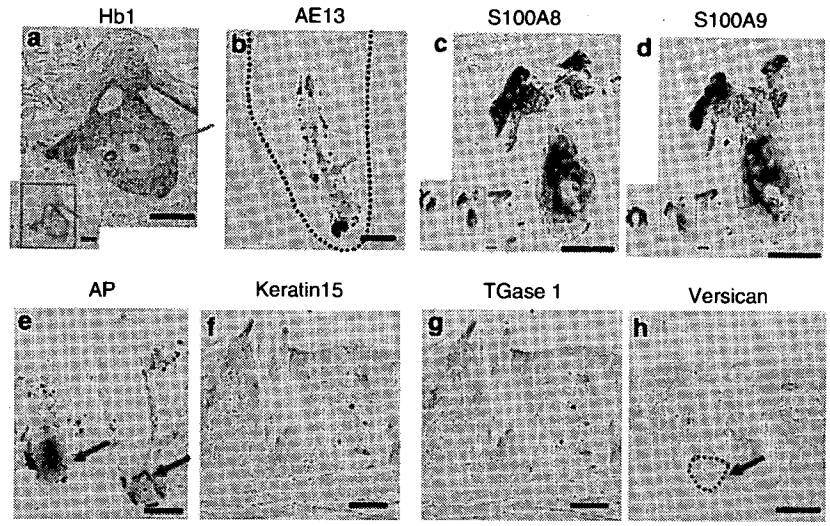

Figure 4. Expression of hair follicle markers in the chimeric hair follicle-like structures (human neonatal keratinocytes/murine DPE). In the hair follicle-like structures generated by co-grafting of human keratinocytes and murine DPE, several markers characteristic of hair follicles were detected: (**a**) hair keratin Hb1 mRNA expression at epithelium (indicated by an arrow), (**b**) hair keratin-specific AE13 immunostaining in the most central layer (indicated by an arrow), (**c**) S100A8 and (**d**) S100A9 mRNA expressions in the epithelium, and (**e**) alkaline phosphatase (AP) activity at the bottom (indicated by arrows and dotted line). The AP activity indicates the nature of DP. Views with lower magnification are also shown for (**a**), (**c**), and **d**, showing the signals were well confined in the epithelium of the structures but were absent from the interfollicular epidermis. However, the expression of either (**f**) keratin15, (**g**) transglutaminase1or (**h**) versican was absent, proteins that are expressed in mature human hair follicles. The blue arrow and dotted line in h indicates presumable DP. Bar (**a**) = 100 μm, (**b–d**) = 50 μm, (**e–h**) = 100 μm.

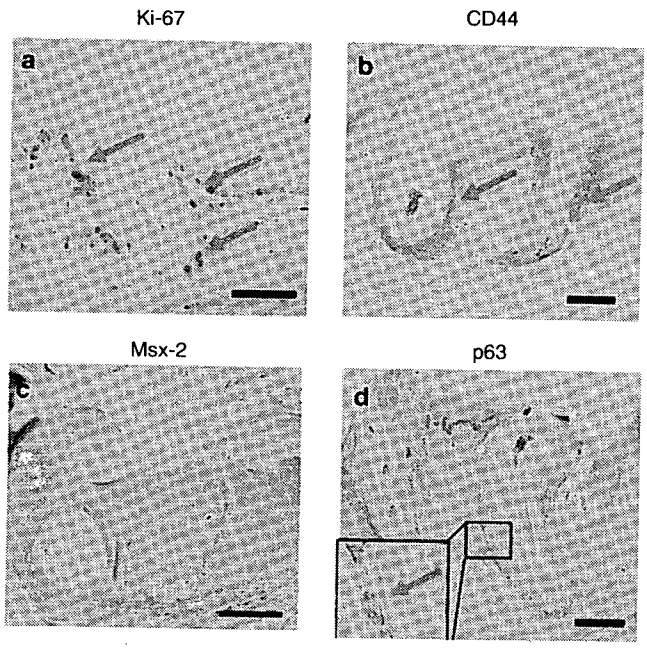

Figure 5. Molecular markers expressed during hair development are detected in the chimeric hair follicle-like structures (human neonatal keratinocytes/murine DPE). The expression of molecular markers known to be expressed during hair development was determined. In the epithelium of the hair follicle-like structures, immunostaining showed: (**a**) a sparse but clear signal for Ki67 within cells at the outermost layer, (**b**) a CD44 signal at the cell periphery of the outer cell layers, (**c**) Msx-2 expression in the inner layers, and (**d**) p63 expression in cells at the outermost follicular epithelium. Bar = 100 μm.

nents of glabrous tissue origin can interact with each other and may form follicular structures.

The chimeric hair follicle-like structures generated in this study exhibit not only morphological similarity but also share expression of some molecular markers with human hair follicles. In normal human hair follicles, hair keratin Hb1 mRNA accumulates in the cortex of mature follicles (Regnier *et al.*, 1997) and AE13 is expressed at the medulla-cortex (Bertolino *et al.*, 1990; Lynch *et al.*, 1986) (also Figure S2a and b). Transcripts for S100A8 and S100A9, multifunctional secreted proteins belonging to the S100 calcium-binding protein family, are abundantly expressed in the medulla of hair shafts and are rarely observed in non-pathological interfollicular epidermis (Schmidt *et al.*, 2001). In our hair follicle-like structures, mRNAs for Hb1, S100A8, and S100A9 were observed in the epithelium, and the signals were confined well within the hair follicle-like structures and are distinct from the surrounding interfollicular epidermis. Immunostaining of AE13 at the innermost area seems in good accordance with the hair shaft of normal hair follicles. The relatively faint signals might be attributed to the incomplete structures as hair shafts. These results imply that human glabrous keratinocytes differentiate into the follicular epithelium. The alkaline phosphatase activity in the DP-like structures also suggests that they are in the early mesenchymal condensation process (Handjiski *et al.*, 1994).

However, these chimeric hair follicle-like structures lack some characteristic features of mature human hair follicles. Neither a bulge region (known as the follicle stem cell reservoir), nor a regular follicular epithelial layer formation

Table 2. Comparison of chimeric hair follicle-like structure features with normal hair follicles

Structure/Marker	Chimeric hair follicle-like structures	Mouse hair follicles	Human hair follicles
Dermal condensation	+	+	+
Epithelial layer formation	±	+	+
Bulge structure	−	+	+
Hair fiber (medulla pattern[1])	± (Solid)	+ (Banded)	+ (Solid)
Alkaline phosphatase (DP)	+	+[2,a]	+[2,b]
Versican (DP)	−	+[2,c,d]	+[c,e]
Hb1 (hair keratin) mRNA	+	NA	+[2,f]
AE13 (hair keratin)	±	+[g]	+[2,g,h]
Keratin 15	−	+[i]	+[2,j]
Transglutaminase 1	−	+[k]	+[2,l]
S100A8 mRNA	+	NA	+[m]
S100A9 mRNA	+	NA	+[m]
Ki67	+	+[n]	+[2]
CD44	+	+[o,p]	+[q]
Msx-2	±	+[r,s]	+[t]
p63	±	+[u]	+[v]

Morphological features and marker expressions of the generated chimeric follicle-like structures are compared with mouse and human normal hair follicles. The formation or expression is indicated as +, observed; ±, faintly observed; −, not observed; NA, data not available.
[1]Medulla patterns are indicated in parenthesis as "banded" or "solid", which is characteristic to mouse or human, respectively.
[2]Staining results are provided as in Figure S2.
References: [a]Handjiski *et al.* (1994); [b]Wong (1968); [c]du Cros *et al.* (1995); [d]Kishimoto *et al.* (1999); [e]Soma *et al.* (2005); [f]Regnier *et al.* (1997); [g]Bertolino *et al.* (1990); [h]Lynch *et al.* (1986); [i]Liu *et al.* (2003); [j]Lyle *et al.* (1998); [k]Tarcsa *et al.* (1997); [l]Thibaut *et al.* (2005); [m]Schmidt *et al.* (2001); [n]Magerl *et al.* (2001); [o]Underhill (1993); [p]Yu and Toole (1997); [q]Seelentag *et al.* (1996); [r]Ma *et al.* (2003); [s]Reginelli *et al.* (1995); [t]Stelnicki *et al.* (1997); [u]Mills *et al.* (1999); [v]Tsujita-Kyutoku *et al.* (2003).

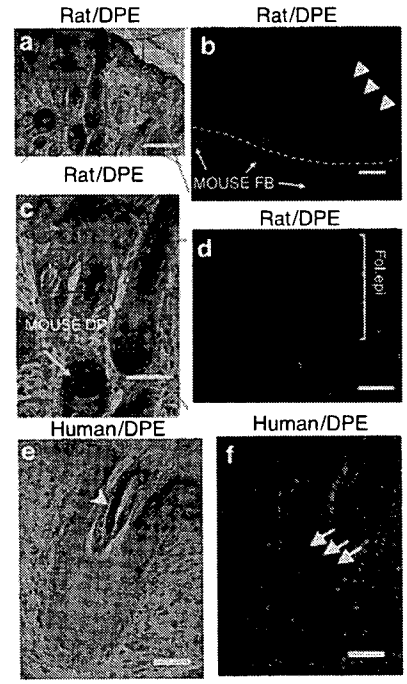

Figure 6. Adult epidermal cells can also generate chimeric hair follicle-like structures (rat or human adult keratinocytes/murine DPE). Chimeric hair follicle-like structures generated from adult keratinocytes with murine DPE cells. (**a–d**) Adult rat keratinocytes were incorporated into both (**a**, **b**) epidermis and (**a**, **c**, **d**) follicular epithelia. FB, fibroblast; DP, dermal papilla. (**e**, **f**) Adult human foreskin-derived keratinocytes also formed the hair follicle-like structures. Keratinized hair shaft-like structure (arrowhead in **e**) was also observed. (**a**, **c**, **e**) HE-staining. (**b**, **d**, **f**) Hoechst 33258 staining: note that uniform nuclear staining indicates non-murine cells (arrowheads in **b**, arrows in **f**) in epithelia, in contrast to bright multinuclear staining for surrounding murine cells from host. Bar (**a**) = 100 μm, (**b**) = 20 μm, (**c**) = 50 μm, (**d**) = 20 μm, (**e**, **f**) = 100 μm.

(i.e. outer root sheath, inner root sheath, cuticle, cortex, and medulla) was observed. Specific markers in more differentiated parts of hair follicles were also missing: keratin15 for bulge and lower outer root sheath (Lyle *et al.*, 1998) and transglutaminase for keratinocyte terminal differentiation (Thibaut *et al.*, 2005). Despite the signs of early mesenchymal condensation (alkaline phosphatase activity as described above), the DP-like structures failed to express versican, which is an anagen DP marker in human and mouse (du Cros *et al.*, 1995; Kishimoto *et al.*, 1999; Soma *et al.*, 2005). This may suggest an inactive status of DP cells that are insufficient to sustain further folliculogenesis. It appears that the initial follicle formation occurs but that the differentiation process is disturbed. EMI between human epidermal cells and mouse DP cells may function to a certain extent but are not sufficient to develop complete hair follicles unlike the recombination with rat epidermal cells. The incomplete hair formation in human/mouse xenografts may also result from differences between hairy (rat) and glabrous (human) skin that the epidermal cells originated from, and/or a possible regression of the hair follicle stem-like nature of keratinocytes during culture (human), in contrast to freshly dissociated epidermal cells (rat).

Although no exclusive hair placode marker is known, several molecules are reported to be expressed during hair development and they are considered as relatively characteristic to the developmental status of the hair follicle. Ki67, a general marker of cellular proliferation, is expressed around hair bulbs, developing outer root sheath and epidermis at early anagen (stage 4), and is eventually concentrated in matrix cells and in very distal outer root sheath in the mature stage (stage 8) (Magerl *et al.*, 2001) (also Figure S2e). CD44, a putative hyaluronan receptor, is expressed in the dermal condensation at an early stage of folliculogenesis, and is then transiently expressed in the follicular epithelium region in the course of development (Underhill, 1993; Yu and Toole, 1997). The transcription factor Msx-2 is expressed in the matrix and precortical cells at early anagen, and expands into the hair cortex and medulla as well in the course of development (Reginelli *et al.*, 1995; Stelnicki *et al.*, 1997; Ma *et al.*, 2003). p63 is a marker for basal and suprabasal cells of the hair follicle including the placode, which plays a

role in epidermal stratification and hair follicle neogenesis (Mills *et al.*, 1999; Zheng *et al.*, 2005). These molecular markers were also detected in the hair follicle-like structures. Expression of Ki67 at the outermost cell layers implies similarity to the early anagen expression pattern rather than mature follicles. These observations may support our assumption that their differentiation process ceases prematurely.

Adult epidermis also generated the chimeric hair follicle-like structures, although the efficiency seemed to be lower than newborn foreskins. This implies that there are only a small number of undifferentiated stem-like cells that have the potential to differentiate into follicular epithelium, and that number decreases with maturation. Whereas even human keratinocytes derived from adult skin were able to differentiate into follicular epithelia with murine DPE, they lost that ability after the second passage. Thus, their ability to differentiate into the follicular epithelium seems to be affected by cellular senescence more than by actual aging. As mentioned earlier, the quantity of cells is also important to exert hair follicle formation (in murine). To prepare sufficient numbers of cells, it will be necessary to establish epidermal cell culture methods without the loss of this differentiation ability.

To reconstitute human hair follicles that are not chimeric with other species, human DP cells with an inductive property will be needed. In contrast to human foreskin keratinocytes that are capable of forming human follicle-like structures together with mouse DPE cells, substitution of a dermal source for human DP cells (primary or P1) failed to show any sign of follicular generation. Only a trace of necrotic DP remained and there was complete replacement of human keratinocytes with host murine keratinocytes (data not shown). As the number of DP cells obtained from human tissues by mechanical dissection is limited, human DP cells had to be expanded in culture by outgrowth from isolated DPs. Their hair inductivity may have been lost by the time of grafting. Identifying suitable culture conditions and/or factors required to maintain the inductive property are high priorities for investigation.

In conclusion, our results show that hair follicle-like structures consisting of human keratinocytes and murine mesenchymal cells are generated. This indicates that EMI function to a certain extent even between human and mouse cells. We have also demonstrated that keratinocytes from glabrous skin can differentiate into follicular epithelia.

MATERIALS AND METHODS

Tissue donors and recipients

Human scalp tissues and neonatal foreskins were obtained from the NDRI/HAB organization with approval of the Ethical Committees of the Shiseido Research Center and the NDRI/HAB organization. Adult foreskins were provided from the phimosis patients with informed consent upon approval of the Ehime University Ethical Committee. Postmortem tissues were excised within 24 hours. All tissues were used for experiments within 72 hours after collection. The study was conducted according to the Declaration of Helsinki Principles. Pregnant ICR mice and IGS rats were purchased from Charles River Japan (Atsugi, Japan). Generation of versican-GFP transgenic mice for the enrichment of DP cells was as described previously (Kishimoto *et al.*, 1999). Nude mice (balb/c, nu/nu) were purchased from Hoshino (Yashio, Japan) and were housed for 1 week before the experiments. All animal procedures had the approval of the Ethical Committee of the Shiseido Research Center.

Preparation of DPE fractions and epidermal cell fractions in rodents

Dorsal skins of newborn (1–3-day-old) ICR mice, versican-GFP transgenic mice or IGS rats were dissected and floated on a 0.25% trypsin solution (GIBCO/BRL, Grand Island, NY) for 16–20 hours at 4°C, after which the epidermis and dermis were separated. The dermis was minced and incubated with 0.35% collagenase in DMEM for 1 hour at 37°C with gentle stirring to dissociate cells. Debris and remaining preformed follicles were removed through the sequential use of 100- and 70-μm cell strainers (BD Pharmingen, Franklin Lakes, NJ). Cells were collected by centrifugation (900 *g*) and were resuspended in Cell Banker II (Nippon Zenyaku Kogyo Co, Tokyo, Japan) at a concentration of 1×10^7 cells/ml and were cryopreserved for more than a week. The viability of cryopreserved cells after 1 month was 72%. These cryopreserved dermal cells were used as the DP-enriched fraction (DPE). The fractions derived from versican-GFP mice were labeled with the nonviable cell-specific marker 7-AAD (Beckman Coulter Inc., Fullerton, CA) and an epithelial-specific monoclonal antibody to CD49f (Serotec Co., Ltd, Sapporo, Japan), then the cellular composition was determined by flow cytometry (EPICS XL-MCL system, Beckman Coulter Inc.). Epidermal sheets were minced and incubated in keratinocyte serum-free (KSF) medium (GIBCO/BRL) for 1 hour at 4°C with gentle stirring. Debris and remaining preformed follicles were removed using the 70-μm cell strainer. Cells were collected by centrifugation (900 *g*) and were resuspended in KSF medium and used for cellular grafting.

Cellular grafting for reconstitution of hair follicles

The cellular grafting procedure for hair follicle reconstitution *in vivo* was performed as described previously (Kishimoto *et al.*, 1999). Briefly, epidermal cell and DP cell fractions (containing 1×10^6–10^7 cells each) were resuspended individually or mixed together in 100 μl of medium, and were then transferred to grafting chambers implanted on the dorsal skins of nude mice (bulb/c, nu/nu). The chambers were removed 1 week after grafting, and hair follicle formation was assessed at 3–4 weeks. Part of each grafting site was dissected for histological observation.

Human keratinocyte culture

Keratinocytes were prepared as described elsewhere (Shirakata *et al.*, 2000). Briefly, neonatal or adult foreskins were cut into 1×1 cm pieces and floated on 400 U/ml purified Dispase I (Godo-Shusei, Tokyo, Japan) in KSF medium for 16–20 hours at 4°C, after which the epidermis was separated from the dermis. The epidermal sheets were incubated in 0.05%–0.53 mM trypsin-EDTA solution (GIBCO/BRL) for 15 minutes at 37°C, and the enzyme was inactivated by adding soybean trypsin inhibitor (2.5 mg/ml). The stratum corneum and other debris were removed by filtration (70 μm). Cells were collected by centrifugation (900 *g*) and cultured in KSF medium supplemented with 0.05 mM $CaCl_2$, bovine pituitary extract, and epidermal growth factor on collagen I- or collagen

IV-coated dishes with an initial cell density of 5×10^3 cells/cm^2. Cells were subcultured when they achieved subconfluence.

Histological observations

Grafts were carefully dissected and fixed in 10% neutral-buffered formalin for 48 hours at ambient temperature, processed through a standard paraffin embedding protocol, and cut into 4–5-μm-thick sections. Sections were processed for routine hematoxylin-eosin histochemistry (H&E staining). For grafts forming the chimeric hair follicle-like structures, the density of the structures was estimated as follows. The total number of the structures in a set of three non-overlapping sections (corresponding to 3 cm length approximately) was counted in three different sets of sections, and the mean value for each recipient was obtained. To evaluate cluster density, the chimeric hair follicle-like structures were divided into "isolated" or "clustered", according to their distance from the nearest adjacent one. When the distance was <0.4 mm, it was counted as "clustered", otherwise as "isolated". The number of chimeric hair follicle-like structures in a cluster was also counted. Results are presented as means$\pm$SD of each condition. Nuclear staining to distinguish mouse cells from rat or human cells was also performed using Hoechst 33258 following a previously described procedure (Ferraris *et al.*, 1997).

Immunohistochemistry

Samples were embedded in OCT compound (Miles Inc., Elkart, IN), or in paraffin after fixation in phosphate-buffered formalin (pH 7.2) for 1 week. Either paraffin or frozen sections were incubated with primary antibodies overnight at 4°C. Immunostaining was visualized using the biotin–streptavidin–peroxidase procedure with TrueBlue™ peroxidase substrate (Kirkegaad & Perry Laboratories Inc., Gaithersburg, MD), followed by counterstaining with nuclear fast red (Sigma, St Louis, MO). Primary antibodies used in this study were: mouse anti-Ki67 monoclonal (BD Bioscience Pharmingen, San Diego, CA), rabbit anti-versican polyclonal (beta-chain; Chemicon, Temecula, CA), rat anti-CD44 monoclonal (Chemicon), mouse anti-p63 monoclonal (BD Pharmingen), rabbit anti-Msx-2 polyclonal (Santa Cruz Biotechnology Inc., Santa Cruz, CA), mouse anti-transglutaminase 1 monoclonal (Harbor bio-products, Norwood, MA), and chicken anti-keratin 15 polyclonal (Covance Research Product Inc., Denver, PA). The antibody recognizing hair keratin (AE13) was a kind gift from T.T. Sun (New York University, New York, NY).

Alkaline phosphatase staining

Frozen sections were fixed in acetone for 10 minutes, washed in phosphate-buffered saline with 0.2% Tween 20 (pH 7.2–7.5), and incubated for 15 minutes in developing solution (BM purple AP substrate, Roche, Indianapolis, IN) (Handjiski *et al.*, 1994).

In situ hybridization

Polymerase chain reaction-derived riboprobe templates were synthesized by introducing the T7 promoter into sense and antisense templates as described previously (Sitzmann and LeMotte, 1993). Gene-specific primer pairs used were as follows: Hb1: ttaggcaccccaa ctca (forward) and aaggggagaggcaggaa (reverse); S100A8 (Marionnet *et al.*, 2003): gggcaagtccgtgggcatcatgttg (forward) and ccagtaactcagc tactctttgggctttct (reverse); S100A9 (Marionnet *et al.*, 2003): gctcctcgg ctttgggacagagtgcaag (forward) and gcatttgtgtccaggtcctccatgatgtgt (reverse). These templates were used to synthesize digoxigenin-labeled RNA probes by *in vitro* transcription with T7 RNA polymerase. The Alu-positive control probe was purchased from Ventana Medical Systems Inc. (Tucson, AZ). *In situ* hybridization was performed on 4-μm sections of 10% formalin-fixed, paraffin-embedded graft tissues. An automated slide-processing system (Discovery™, Ventana Medical Systems Inc., Tucson, AZ, USA) was used (Nitta *et al.*, 2003) with protocols based on the standard protocol described in the RiboMap™ application note. Signals were detected automatically using the BlueMap™ NBT/BCIP substrate kit for 3 hours at 37°C.

CONFLICT OF INTEREST

The authors state no conflict of interest.

ACKNOWLEDGMENTS

We thank T.T. Sun at NY State University for his kind gift of the AE13 antibody. This work was partly supported by a grant for scientific research from the Ministry of Education, Culture, Sports, Science, and Technology of Japan and by a grant for Research on Specific Disease from the Ministry of Health, Labour, and Welfare of Japan.

SUPPLEMENTARY MATERIAL

Figure S1. Xenotypic cellular grafting between murine and rat cells.

Figure S2. Expression of hair follicle markers in normal hair follicles.

REFERENCES

Bertolino AP, Checkla DM, Heitner S, Freedberg IM, Yu DW (1990) Differential expression of type I hair keratins. *J Invest Dermatol* 94:297–303

Blanpain C, Lowry WE, Geoghegan A, Polak L, Fuchs E (2004) Self-renewal, multipotency, and the existence of two cell populations within an epithelial stem cell niche. *Cell* 118:635–48

du Cros DL, LeBaron RG, Couchman JR (1995) Association of versican with dermal matrices and its potential role in hair follicle development and cycling. *J Invest Dermatol* 105:426–31

Ferraris C, Bernard BA, Dhouailly D (1997) Adult epidermal keratinocytes are endowed with pilosebaceous forming abilities. *Int J Dev Biol* 41: 491–8

Ferraris C, Chevalier G, Favier B, Jahoda CA, Dhouailly D (2000) Adult corneal epithelium basal cells possess the capacity to activate epidermal, pilosebaceous and sweat gland genetic programs in response to embryonic dermal stimuli. *Development* 127:5487–95

Ghali L, Wong ST, Tidman N, Quinn A, Philpott MP, Leigh IM (2004) Epidermal and hair follicle progenitor cells express melanoma-associated chondroitin sulfate proteoglycan core protein. *J Invest Dermatol* 122:433–42

Handjiski BK, Eichmuller S, Hofmann U, Czarnetzki BM, Paus R (1994) Alkaline phosphatase activity and localization during the murine hair cycle. *Br J Dermatol* 131:303–10

Hardy MH (1992) The secret life of the hair follicle. *Trends Genet* 8: 55–61

Hashimoto T, Kazama T, Ito M, Urano K, Katakai Y, Yamaguchi N *et al.* (2000) Histologic and cell kinetic studies of hair loss and subsequent recovery process of human scalp hair follicles grafted onto severe combined immunodeficient mice. *J Invest Dermatol* 115: 200–6

Jahoda CA, Oliver RF, Reynolds AJ, Forrester JC, Horne KA (1996) Human hair follicle regeneration following amputation and grafting into the nude mouse. *J Invest Dermatol* 107:804–7

Kamimura J, Lee D, Baden HP, Brissette J, Dotto GP (1997) Primary mouse keratinocyte cultures contain hair follicle progenitor cells with multiple differentiation potential (published erratum appears in *J Invest Dermatol* 1998 **110**(1):102). *J Invest Dermatol* 109:534–40

Kishimoto J, Ehama R, Wu L, Jiang S, Jiang N, Burgeson RE (1999) Selective activation of the versican promoter by epithelial- mesenchymal interactions during hair follicle development. *Proc Natl Acad Sci USA* 96:7336–41

Li A, Simmons PJ, Kaur P (1998) Identification and isolation of candidate human keratinocyte stem cells based on cell surface phenotype. *Proc Natl Acad Sci USA* 95:3902–7

Lichti U, Weinberg WC, Goodman L, Ledbetter S, Dooley T, Morgan D *et al.* (1993) *In vivo* regulation of murine hair growth: insights from grafting defined cell populations onto nude mice. *J Invest Dermatol* 101:124S–9S

Liu Y, Lyle S, Yang Z, Cotsarelis G (2003) Keratin 15 promoter targets putative epithelial stem cells in the hair follicle bulge. *J Invest Dermatol* 121:963–8

Lyle S, Christofidou-Solomidou M, Liu Y, Elder DE, Albelda S, Cotsarelis G (1998) The C8/144B monoclonal antibody recognizes cytokeratin 15 and defines the location of human hair follicle stem cells. *J Cell Sci* 111(Part 21):3179–88

Lynch MH, O'Guin WM, Hardy C, Mak L, Sun TT (1986) Acidic and basic hair/nail ("hard") keratins: their colocalization in upper cortical and cuticle cells of the human hair follicle and their relationship to "soft" keratins. *J Cell Biol* 103:2593–606

Ma L, Liu J, Wu T, Plikus M, Jiang TX, Bi Q *et al.* (2003) "Cyclic alopecia" in Msx2 mutants: defects in hair cycling and hair shaft differentiation. *Development* 130:379–89

Magerl M, Tobin DJ, Muller-Rover S, Hagen E, Lindner G, McKay IA *et al.* (2001) Patterns of proliferation and apoptosis during murine hair follicle morphogenesis. *J Invest Dermatol* 116:947–55

Marionnet C, Bernerd F, Dumas A, Verrecchia F, Mollier K, Compan D *et al.* (2003) Modulation of gene expression induced in human epidermis by environmental stress *in vivo*. *J Invest Dermatol* 121:1447–58

Millar SE (2002) Molecular mechanisms regulating hair follicle development. *J Invest Dermatol* 118:216–25

Mills AA, Zheng B, Wang XJ, Vogel H, Roop DR, Bradly A (1999) p63 is a homologue required for limb and epidermal morphogenesis. *Nature* 398:708–13

Morris RJ, Liu Y, Marles L, Yang Z, Trempus C, Li S *et al.* (2004) Capturing and profiling adult hair follicle stem cells. *Nat Biotechnol* 22:411–7

Nitta H, Kishimoto J, Grogan TM (2003) Application of automated mRNA *in situ* hybridization for formalin-fixed, paraffin-embedded mouse skin sections: effects of heat and enzyme pretreatment on mRNA signal detection. *Appl Immunohistochem Mol Morphol* 11:183–7

Reginelli AD, Wang YQ, Sassoon D, Muneoka K (1995) Digit tip regeneration correlates with regions of Msx1 (Hox 7) expression in fetal and newborn mice. *Development* 121:1065–76

Regnier CH, Asch PH, Grosshans E, Rio MC (1997) Expression pattern of human hair keratin basic 1 (hHb1) in hair follicle and pilomatricoma. *Exp Dermatol* 6:87–90

Reynolds AJ, Jahoda CA (2004) Cultured human and rat tooth papilla cells induce hair follicle regeneration and fiber growth. *Differentiation* 72:566–75

Rheinwald JG, Green H (1975) Serial cultivation of strains of human epidermal keratinocytes: the formation of keratinizing colonies from single cells. *Cell* 6:331–43

Schmidt M, Gillitzer R, Toksoy A, Brocker EB, Rapp UR, Paus R *et al.* (2001) Selective expression of calcium-binding proteins S100A8 and S100A9 at distinct sites of hair follicles. *J Invest Dermatol* 117:748–50

Seelentag WK, Gunthert U, Saremaslani P, Futo E, Pfaltz M, Heitz PU *et al.* (1996) CD44 standard and variant isoform expression in normal human skin appendages and epidermis. *Histochem Cell Biol* 106: 283–9

Shimizu H, Morgan BA (2004) Wnt signaling through the beta-catenin pathway is sufficient to maintain, but not restore, anagen-phase characteristics of dermal papilla cells. *J Invest Dermatol* 122:239–45

Shirakata Y, Komurasaki T, Toyoda H, Hanakawa Y, Yamasaki K, Tokumaru S *et al.* (2000) Epiregulin, a novel member of the epidermal growth factor family, is an autocrine growth factor in normal human keratinocytes. *J Biol Chem* 275:5748–53

Sitzmann JH, LeMotte PK (1993) Rapid and efficient generation of PCR-derived riboprobe templates for *in situ* hybridization histochemistry. *J Histochem Cytochem* 41:773–6

Soma T, Tajima M, Kishimoto J (2005) Hair cycle-specific expression of versican in human hair follicles. *J Dermatol Sci* 39:147–54

Stelnicki EJ, Komuves LG, Holmes D, Clavin W, Harrison MR, Adzick NS *et al.* (1997) The human homeobox genes MSX-1, MSX-2, and MOX-1 are differentially expressed in the dermis and epidermis in fetal and adult skin. *Differentiation* 62:33–41

Stenn KS, Paus R (2001) Controls of hair follicle cycling. *Physiol Rev* 81:449–94

Tarcsa E, Marekov LN, Andreoli J, Idler WW, Candi E, Chung S *et al.* (1997) The fate of trichohyalin. Sequential post-translational modifications by peptidyl-arginine deiminase and transglutaminases. *J Biol Chem* 272:27893–901

Thibaut S, Candi E, Pietroni V, Melino G, Schmidt R, Bernard BA (2005) Transglutaminase 5 expression in human hair follicle. *J Invest Dermatol* 125:581–5

Triel C, Vestergaard ME, Bolund L, Jensen TG, Jensen UB (2004) Side population cells in human and mouse epidermis lack stem cell characteristics. *Exp Cell Res* 295:79–90

Tse Y, Cooper KD (1990) Cutaneous dermal Ia+ cells are capable of initiating delayed type hypersensitivity responses. *J Invest Dermatol* 94: 267–72

Tsujita-Kyutoku M, Kiuchi K, Danbara N, Yuri T, Senzaki H, Tsubura A (2003) p63 expression in normal human epidermis and epidermal appendages and their tumors. *J Cutan Pathol* 30:11–7

Underhill CB (1993) Hyaluronan is inversely correlated with the expression of CD44 in the dermal condensation of the embryonic hair follicle. *J Invest Dermatol* 101:820–6

Wong CK (1968) The fine structure of the dermal papilla and electron microscopic localization of alkaline phosphatase in the dermal papilla of the human hair follicle. *Sapporo Igaku Zasshi* 34:1–18

Yu Q, Toole BP (1997) Common pattern of CD44 isoforms is expressed in morphogenetically active epithelia. *Dev Dyn* 208:1–10

Zheng Y, Du X, Wang W, Boucher M, Parimoo S, Stenn K (2005) Organogenesis from dissociated cells: generation of mature cycling hair follicles from skin-derived cells. *J Invest Dermatol* 124: 867–876

Available online at www.sciencedirect.com
ScienceDirect
Biochemical and Biophysical Research Communications 363 (2007) 584–590
BBRC
www.elsevier.com/locate/ybbrc

Involvement of γ-secretase in postnatal angiogenesis ☆

Hiroki Hayashi [a], Hironori Nakagami [a,*], Yoichi Takami [a], Naoyuki Sato [b], Yukihiro Saito [a], Tomoyuki Nishikawa [a], Masaki Mori [a], Hiroshi Koriyama [a], Katsuto Tamai [a], Ryuichi Morishita [b], Yasufumi Kaneda [a]

[a] *Division of Gene Therapy Science, Graduate School of Medicine, Osaka University, 2-2 Yamada-oka, Suita, Osaka 565-0871, Japan*
[b] *Division of Clinical Gene Therapy, Graduate School of Medicine, Osaka University, Osaka 565-0871, Japan*

Received 4 September 2007
Available online 14 September 2007

Abstract

γ-Secretase cleaves the transmembrane domains of several integral membrane proteins involved in vasculogenesis. Here, we investigated the role of γ-secretase in the regulation of postnatal angiogenesis using γ-secretase inhibitors (GSI). In endothelial cell (EC), γ-secretase activity was up-regulated under hypoxia or the treatment of vascular endothelial growth factor (VEGF). The treatment of GSI significantly attenuated growth factor-induced EC proliferation and migration as well as *c-fos* promoter activity in a dose-dependent manner. In vascular smooth muscle cell (VSMC), treatment of GSI significantly attenuated growth factor-induced VEGF and fibroblast growth factor-2 (FGF-2) expression. Indeed, GSI attenuated VEGF-induced tube formation and inhibited FGF-2-induced angiogenesis on matrigel in mice as quantified by FITC-lectin staining of EC. Overall, we demonstrated that γ-secretase may be key molecule in postnatal angiogenesis which may be downstream molecule of growth factor-induced growth and migration in EC, and regulate the expression of angiogenic growth factors in VSMC.

Keywords: Angiogenesis; Endothelial function; γ-Secretase activity; Growth factors; Hypoxia

The γ-secretase complex is a high-molecular-weight complex that consists of at least four different proteins: presenilin1 (PS1) and 2 (PS2), nicastrin, Aph-1 (anterior pharynx defective-1), and Pen-2 (presenilin enhancer-2) [1,2]. This complex cleaves key signaling molecules, including the amyloid precursor protein (APP), Notch, CD44, ErbB-4, and N (neural)- and VE (vascular endothelial)-cadherins [2–5]. Mice lacking the PS1 gene exhibit severe phenotype, characterized by late embryonic lethality which included yolk sac vasculogenesis problems [6,7]. It has been suggested that many of these lesions were a consequence of disturbed Notch signaling in mice [8,9]. γ-Secretase also released Aβ peptides with the proteolysis of the transmembrane domain of APP. Aβ peptides stimulate EC proliferation, migration, and morphogenesis in matrigel [10] and functionally synergize with fibroblast growth factor-2 (FGF-2) to promote angiogenesis *in vivo* [11]. Although VEGF also increases the expression of Notch receptors and their ligands [12], it is still unknown how γ-secretase, regulator of Notch or APP signaling, contributes to VEGF-induced postnatal angiogenesis. The present study investigated the role of γ-secretase in the regulation of angiogenesis by the employing potent γ-secretase inhibitors (GSI).

Materials and methods

Materials and cell culture. The γ-secretase inhibitors (GSI), L-685,458, and (3,5-difluorophenylacetyl)-Ala-Phg-Obu^t (DAPT) were obtained from Peptide Institute, Inc. (Osaka, Japan). HAEC (human aortic endothelial cell), HASMC (human aortic smooth muscle cell), and BAEC (bovine

☆ This work was supported by the Northern Osaka (Saito) Biomedical Knowledge-Based Cluster Creation Project (to Y.K.), and Japan Heart Foundation Grant for Research (to H.N).
* Corresponding author. Fax: +81 6 6879 3909.
E-mail address: nakagami@gts.med.osaka-u.ac.jp (H. Nakagami).

0006-291X/$ - see front matter © 2007 Elsevier Inc. All rights reserved.
doi:10.1016/j.bbrc.2007.09.003

aortic endothelial cell) were purchased from Clonetics Co. (Palo Alto, CA) and A7r5 (smooth muscle obtained from embryonic rat thoracic aorta) were purchased from the American Type Culture Collection (ATCC) that were maintained as previously described [13].

Functional assay. Cell viability was evaluated by a CellTiter 96 Aqueous One Solution Cell Proliferation Assay (MTS) kit (Promega, Madison, WI). Cell proliferation was assessed by thymidine incorporation, and also evaluated using the *c-fos* promoter luciferase activity. The VEGF promoter activity and serum response element (SRE) activity were also measured by luciferase activity after overexpression of these promoter-driven luciferase plasmids. These analyses were performed as previously described [13–15]. HAEC migration was measured using a modified Boyden chamber assay [16]. Aβ40 levels were measured by Aβ sandwich enzyme-linked immunosorbent assay (ELISA) according to the manufacturer's instructions (Wako Pure Chemical Industries, Ltd., Osaka).

Tube formation assay. A HAEC tube formation assay was conducted in triplicate using an Angiogenesis Kit (Kurabo, Osaka), as per the manufacturer's instructions [17]. Briefly, cells were treated with increasing concentrations of GSI (1–10 μM) in the presence of VEGF (10 ng/ml). After 7 days of incubation, cells were stained with monoclonal anti-human CD31 antibody. Stained cells were photographed, and tubule-like structures in the images were analyzed for area, length, path, and joint in tube formation using an Angiogenesis Image Analyzer (Kurabo, Osaka).

In vitro peptide cleavage assay for γ-secretase activity. The measurement of γ-secretase activity was performed as previously described [18]. Briefly, the membrane fraction was isolated, and 10 μg of the supernatants were incubated with 10 μM of fluorescence-conjugated peptide substrate (NMA-GGVVIATVK(DNP)-DRDRDR-NH_2, Peptide Institute, Inc., Osaka) at 37 °C for 16–18 h. The degree of substrate cleavage was measured at an excitation wavelength of 355 nm and an emission wavelength of 440 nm.

Directed in vivo angiogenesis assay (DIVAA). A directed *in vivo* angiogenesis assay (DIVAA; Trevigen, Inc., Gaithersburg, MD) was performed as previously described [19]. All experimental protocols were approved by the Osaka University Graduate School of Medicine Standing Committee on Animals.

Statistical analysis. All values are expressed as means ± SD. Analysis of variance with subsequent Fisher's PLSD test or the unpaired Student's *t* test was employed to determine the significance of differences in multiple comparisons. All statistical analysis was performed using Stat-View 5.0 software (SAS Institute, Inc., NC). Values of $p < 0.05$ were considered to represent statistical significance.

The detail information was described in Supplementary information.

Results

Measurement of γ-secretase activity in EC and SMC

The expression of γ-secretase components, substrates, and downstream genes in HAEC and HASMC were evaluated by RT-PCR. PS1, PS2, Aph-1, nicastrin, Pen-2, CHF2, Hes1, Hes5, and APP were expressed in both vascular cells types. Although most of Notch ligands and receptors were also expressed in both vascular cell types, Notch4 was expressed in only HAEC. And Notch3 was only expressed in HASMC. The downstream target genes of Notch, CHF2, Hes1, 5, and APP were expressed in both cells (Supplementary Fig. 1). Protein expression of γ-secretase components (PS1, PS2, nicastrin, Aph-1, Pen-2) and its related protein (Notch1, APP, Hes1) was also confirmed by Western blot (Fig. 1A).

HAEC and HASMC γ-secretase activity was significantly inhibited by two different kinds of GSI, L-685,458, or DAPT, as assessed by the peptide cleavage assay (in HAEC; 82% inhibition in DAPT 10 μM, 90% inhibition in L-685,458 10 μM, in HASMC; 84% inhibition in DAPT 10 μM, 95% inhibition in L-685,458 10 μM) as shown in Fig. 1B. To further confirm the reliability of γ-secretase activity assay, we examined the effect of GSI on substrates of cleavage by γ-secretase by using pCS2-Notch1ΔE-6myc construct, which contains only γ-secretase cleavage site [20]. Indeed, in the overexpressed pCS2-Notch1ΔE-6myc cells, GSI suppressed production of Notch intracellular variant (ICV) from transmembrane variant (ΔE) compared to DMSO in BAEC and A7r5 (Fig. 1C). These data suggest that GSI, DAPT, and L-685,458, specifically suppress γ-secretase leading to cleavage of substrates in vascular cells.

GSI inhibits EC proliferation and migration

Treatment of HAEC with hypoxia or growth factors significantly increased γ-secretase activity [10% increase by hypoxia, 18% increase by VEGF 10 ng/ml, 26% increase by growth factors (hrVEGF 25 ng/ml, hrFGF-2 25 ng/ml, hrEGF 25 ng/ml) shown in Fig. 2A]. Of importance, endogenous Aβ40 production of HAEC was up-regulated by growth factors (hrVEGF 25 ng/ml, hrFGF-2 25 ng/ml, hrEGF 25 ng/ml) and suppressed by GSI (Supplementary Fig. 2A). In addition, Hes1, target gene of Notch, was up-regulated by hypoxia or growth factors and suppressed by addition of GSI (Supplementary Fig. 2B). These results suggest that angiogenic growth factors and hypoxic condition increase γ-secretase activity, thereby modulating Notch signaling and Aβ production.

The effect of GSI on EC growth was evaluated using the MTS assay and thymidine incorporation assay. Treatment of HAEC with growth factors (hrVEGF 25 ng/ml, hrFGF-2 25 ng/ml, hrEGF 25 ng/ml) increased HAEC viability, and this effect was attenuated by L-685,458 in a dose-dependent manner (121% inhibition, 10 μM). A similar effect was observed with DAPT (110% inhibition, 10 μM) (Fig. 2B). Similarly, HAEC proliferation by thymidine incorporation assay was also inhibited by GSI (86% inhibition in growth factors + L-685,458, 106% inhibition in growth factors + DAPT 10 μM) (Fig. 2C). Use of a modified Boyden chamber assay demonstrated that GSI significantly inhibited growth factors induced-migration of HAEC (67% inhibition in L-685,458 10 μM, and 73% inhibition in DAPT 5 μM) (Fig. 2D and E). Taken together, inhibition of γ-secretase activity suppresses growth factors-induced proliferation and migration in EC.

GSI inhibits c-fos promoter and SRE activity but not Akt and ERK activity in EC

Angiogenic factors usually strongly induce Akt and ERK phosphorylation in EC, leading to an angiogenic effect. Indeed, treatment of HAEC with recombinant growth factors (hrVEGF 25 ng/ml, hrFGF-2 25 ng/ml, hrEGF 25 ng/ml) induced ERK and Akt phosphorylation at 10 min, and

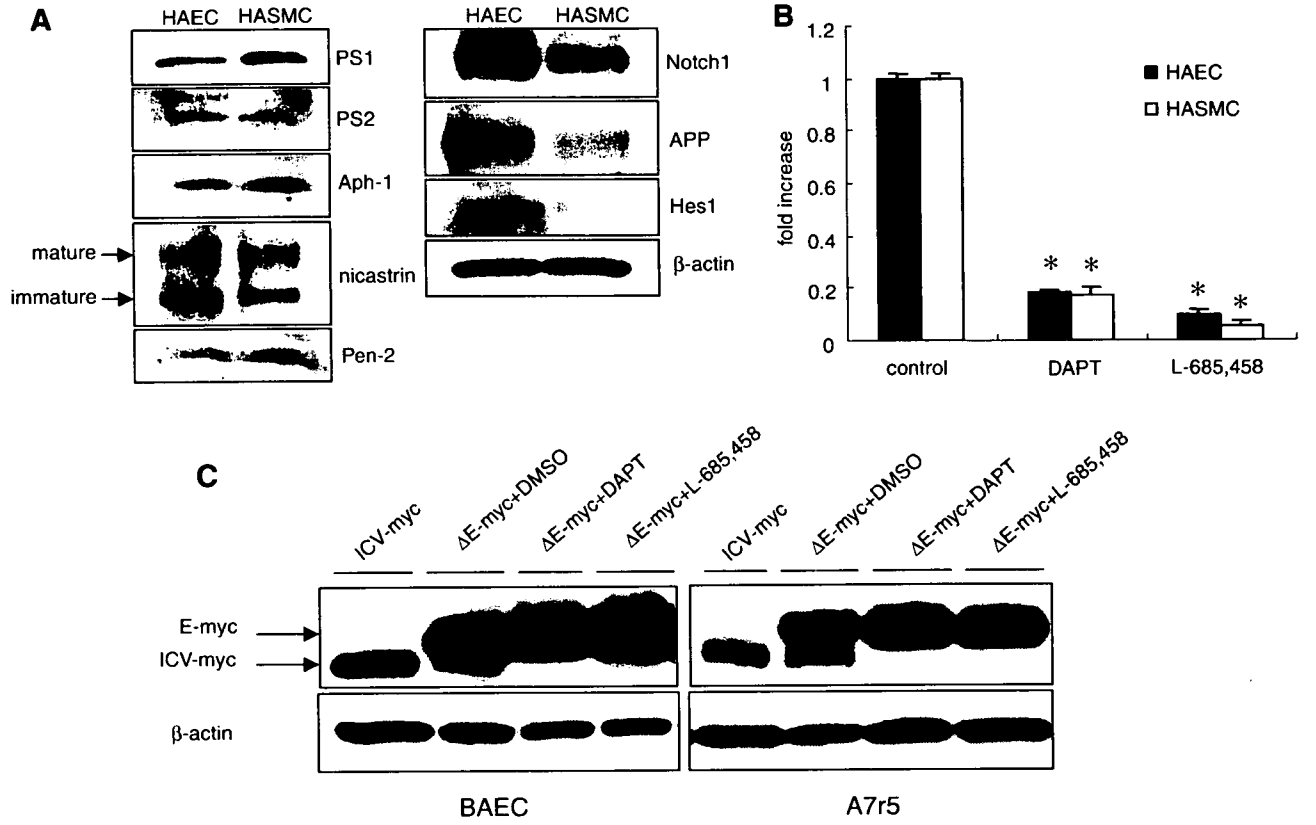

Fig. 1. The expression of γ-secretase related genes, and the γ-secretase inhibition by potent inhibitors. (A) The protein expression of γ-secretase component [presenilin (PS) 1/2, Aph (anterior pharynx defective)-1, nicastrin, Pen (presenilin enhancer)-2], its related proteins, [Notch1, APP (amyloid precursor protein), Hes (hairy/enhancer split gene) 1] were detected by Western blot with β-actin as loading control. (B) The γ-secretase activity in HAEC and HASMC with or without L-685,458 or DAPT. "control" indicates treatment with DMSO. "DAPT" or "L-685,458" indicates treatment with DAPT 10 μM or L-685,458 10 μM for 24 h. $^{*}p < 0.0001$ vs. control, respectively. (C) Analysis of Notch cleavage efficiency in BAEC or A7r5 by Western blot with myc-tag. ΔE indicates the membrane anchored Notch derivative containing γ-secretase cleavage site. ICV (intracellular variant) band indicates the product of cleavage of ΔE by γ-secretase. "ΔE-myc + DMSO" indicates transfection with ΔE-myc and treatment with DMSO as control. "ΔE-myc + DAPT" or "ΔE-myc + L-685,458" indicates transfection with ΔE-myc and treatment with DAPT 10 μM or L-685,458 10 μM, respectively.

pre-treatment with L-685,458 (1 μM, 10 μM) and DAPT (1 μM, 10 μM) had no effect on this phenomenon in HAEC (Fig. 3A). However, pre-treatment of BAEC with L-685,458 or DAPT attenuated recombinant growth factors-induced *c-fos* promoter activity (86% inhibition in L-685,458 10 μM; 72% inhibition in DAPT 10 μM; Fig. 3B). Further, treatment of BAEC with recombinant growth factors resulted in a 1.4-fold increase in SRE promoter activity compared with no treatment, and pre-treatment of L-685,458 and DAPT significantly attenuated this effect (Fig. 3C).

GSI inhibits angiogenesis in vitro and in vivo angiogenesis

In the process of angiogenesis, SMC stimulates the growth of EC by secretion of growth factors, such as VEGF and FGF-2, which can be also induced by growth factor, i.e. PDGF-BB. In HASMC, γ-secretase activity was significantly up-regulated by the treatment with PDGF-BB 10 ng/ml (22% increase, Fig. 4A). Treatment of HASMC with hrPDGF-BB 10 ng/ml also increased the mRNA levels of VEGF and FGF-2, as evaluated by qPCR, and L-685,458 significantly inhibited this effect (76% inhibition in VEGF and 87% inhibition in FGF-2; Fig. 4B). Further, L-685,458 attenuated the PDGF-BB-induced increase in VEGF promoter activity in a dose-dependent manner (66% inhibition in 10 μM L-685,458, Supplementary Fig. 3A).

We further examined the contribution of γ-secretase to the process of HAEC sprouting. Treatment of HAEC with hrVEGF 10 ng/ml strongly induced EC sprouting, as demonstrated by immunostaining with human monoclonal anti-CD31 antibody, and this effect was attenuated by GSI. Quantitative analyses revealed that L-685,458 inhibited multiple parameters of hrVEGF-induced tube formation (1 μM, 71% inhibition in length and 71% inhibition in area; 10 μM, 93% inhibition in length, 91% inhibition in area, 76% inhibition in path, 64% inhibition in joint). Another GSI (DAPT 10 μM) produced similar results (Fig. 4C and D).

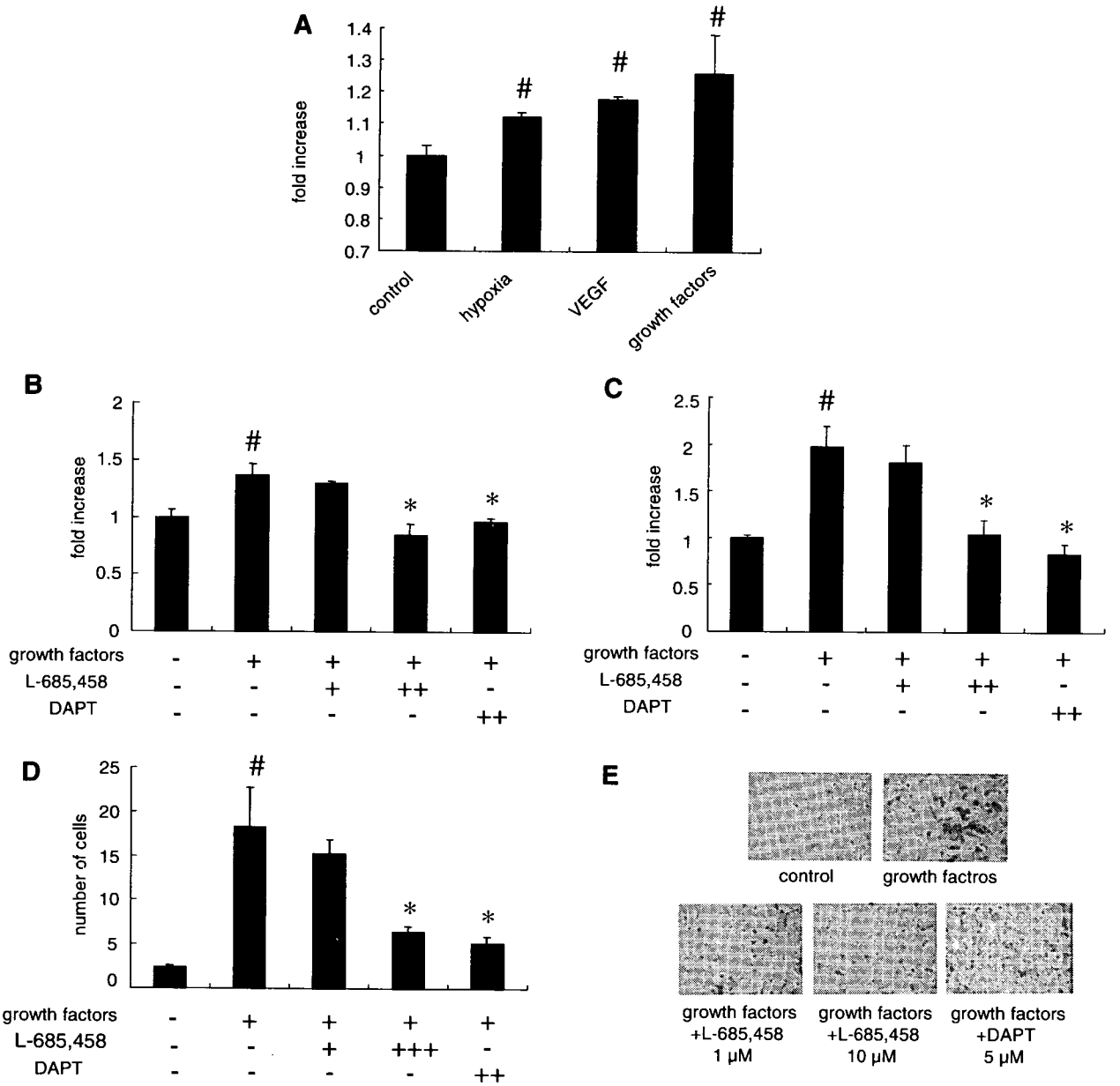

Fig. 2. Measurement of γ-secretase activity, and the enhance effect of hypoxia or growth factors and the inhibitory effect of GSI on proliferation and migration of EC. (A) γ-Secretase activity of HAEC treated with or without hypoxia or growth factors. "control" indicates no treatment. "hypoxia" indicates treatment with hypoxia. "VEGF" indicates treatment with hrVEGF 10 ng/ml. "growth factors" indicates treatment with hrVEGF 25 ng/ml, hrFGF-2 25 ng/ml and hrEGF 25 ng/ml. $^{\#}P < 0.01$ vs. control (B) Cell viability of HAEC by MTS assay treated with L-685,458 (+ = 1 μM, ++ = 10 μM) or DAPT (++ = 10 μM) in the presence of growth factors (hrVEGF 25 ng/ml, hrFGF-2 25 ng/ml, hrEGF 25 ng/ml) as determined by MTS assay. $^{\#}p < 0.01$ vs. control. $^{*}p < 0.01$ vs. growth factors. (C) The effect on DNA synthesis by thymidine incorporation in HAEC treated with of GSI, L-685,458 (+ = 1 μM, ++ = 10 μM) or DAPT (++ = 10 μM), in the presence of growth factors (hrVEGF 25 ng/ml, hrFGF-2 25 ng/ml, hrEGF 25 ng/ml) was analyzed by ^{3}H thymidine incorporation assay. $^{\#}p \leq 0.01$ vs. no treatment. $^{*}p < 0.005$ vs. treatment with growth factors. (D) Migration of HAEC treated with growth factors in the presence or absence of GSI (L-685,458 + = 1 μM, +++ = 10 μM; DAPT ++ = 5 μM). "growth factors" indicates treatment with hrVEGF 50 ng/ml, hrFGF-2 50 ng/ml, and hrEGF 50 ng/ml. $^{*}p < 0.01$ vs. no treatment. $^{\#}p < 0.01$ vs. treatment with "growth factors". (E) Representative pictures of migrated cells stained with blue (200× magnification) in the presence or absence of GSI (L-685,458 1 or 10 μM; or DAPT 5 μM). "control" indicates treatment with no treatment (DMSO), "growth factors" indicates treatment with hrVEGF 50 ng/ml, hrFGF-2 50 ng/ml, and hrEGF 50 ng/ml.

Next, we investigated the effect of GSI on *in vivo* angiogenesis. DIVAA demonstrated that neovessel formation in rFGF-2 incorporated matrigel, and quantitative analysis of FITC-lectin stained cells showed that rFGF-2 significantly induced neovessels. Co-incorporation of L-685,458 significantly inhibited rFGF-2-induced neovessels

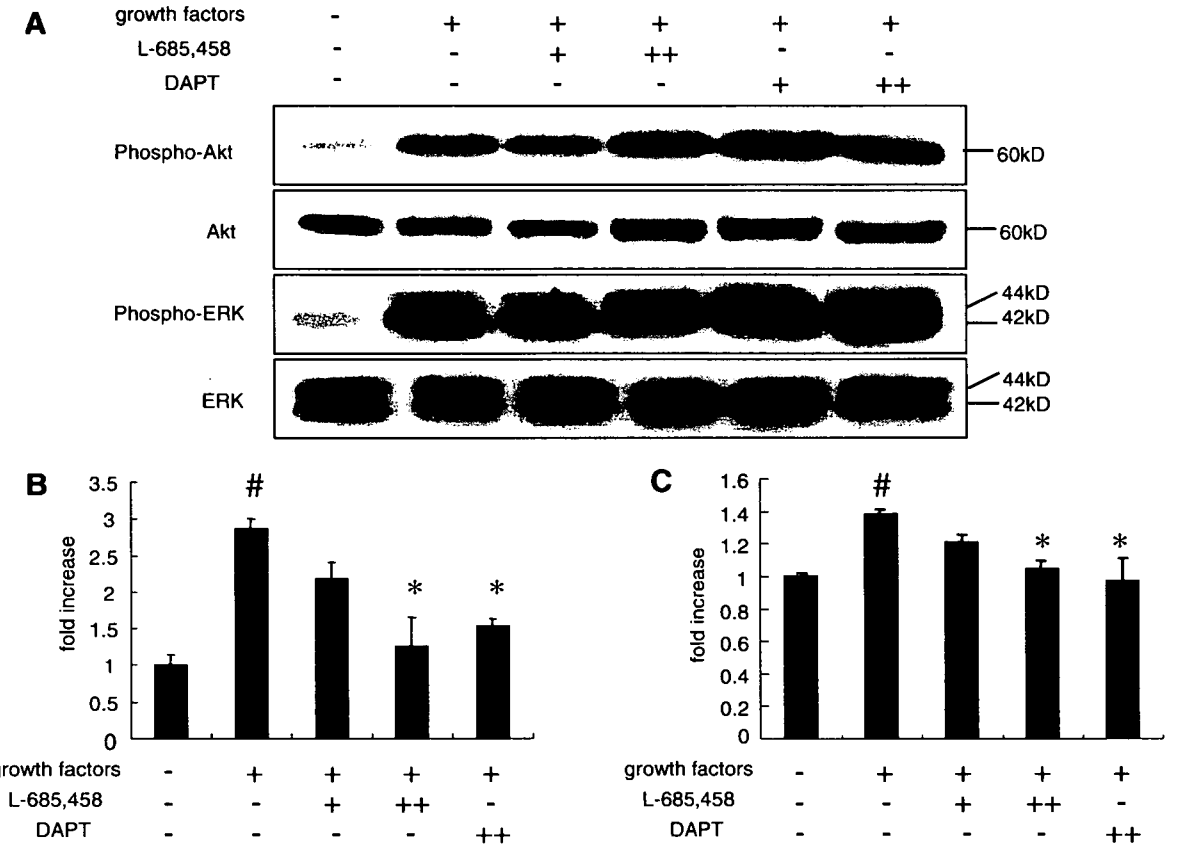

Fig. 3. GSI suppressed SRE- and *c-fos* promoter activity, but not the Akt and ERK signaling pathway. (A) Western blotting of HAEC pretreated with or without GSI, L-685,458 (+ = 1 μM, ++ = 10 μM) or DAPT (+ = 1 μM, ++ = 10 μM), in the presence of growth factors (hrVEGF 25 ng/ml, hrFGF-2 25 ng/ml, hrEGF 25 ng/ml). Upper two panels show phosphospecific Akt (phospho-Akt) and total Akt (Akt), and lower two panels show phosphospecific-ERK (phospho-ERK) and total ERK (ERK). "growth factors" indicates treatment with hrVEGF 25 ng/ml, hrFGF-2 25 ng/ml, and hrEGF 25 ng/ml. (B) The effect of GSI on *c-fos*-promoter activity induced by growth factors. BAEC was treated with GSI (L-685,458 + = 1 μM, ++ = 10 μM, DAPT ++ = 10 μM) in the presence of "growth factors" (hrVEGF 25 ng/ml, hrFGF-2 25 ng/ml, hrEGF 25 ng/ml). $^{\#}p < 0.01$ vs. no treatment. $^{*}p < 0.01$ vs. treatment with growth factors. (C) Effect of GSI on SRE-promoter activity induced by growth factors. BAEC was treated with GSI (L-685,458 + = 1 μM, ++ = 10 μM, DAPT ++ = 10 μM) in the presence of "growth factors" (hrVEGF 25 ng/ml, hrFGF-2 25 ng/ml, hrEGF 25 ng/ml). $^{\#}p < 0.01$ vs. no treatment. $^{*}p < 0.01$ vs. treatment with growth factors.

(27% inhibition, $p < 0.05$; Fig. 4E and F). These results suggest that inhibition of γ-secretase has an anti-angiogenic effect *in vivo*.

Discussion

The present study demonstrated that GSI attenuated postnatal angiogenesis through inhibition of EC growth and expression of angiogenic growth factors. In human arterial EC, VEGF-induced up-regulation of Notch1 and its ligand, Dll4 [12], and were shown to play a role in vascular development downstream of Notch [21]. These results suggest a crucial role for Notch signaling in vasculogenesis. However, Notch activity down-regulates VEGFR2 expression, and Notch signaling acts to counteract the proliferative drive [22,23]. Thus, Notch signaling may be somehow complicated in adult angiogenesis because several downstream targeted genes have bi-directional activity in the process of tissue remodeling. Takeshita et al. recently described the essential role of Notch signaling in EC in the process of embryonic and postnatal angiogenesis by using EC-specific deficient mice [24]. Similarly, the present study suggests that γ-secretase or substrates/products of this enzyme play a critical role in angiogenesis. However, while *c-fos* promoter and SRE activity were inhibited by GSI, neither ERK nor Akt phosphorylation was affected by treatment with GSI. Thus, a γ-secretase-dependent transcription factor, such as Hes or CHF family, may mediate the transcriptional regulation of angiogenesis-related genes. In addition, Aβ peptides which were released by the cleavage of APP by γ-secretase may contribute to the part of postnatal angiogenesis [6,7,25,26].

In this study, γ-secretase activity was up-regulated under the treatment of hypoxic condition and/or angiogenic growth factors. Indeed, it has been reported that activation of hypoxia inducible factor (HIF)-1 dramatically increased Aph-1 expression, which is a major component of the γ-secretase complex, accompanied by

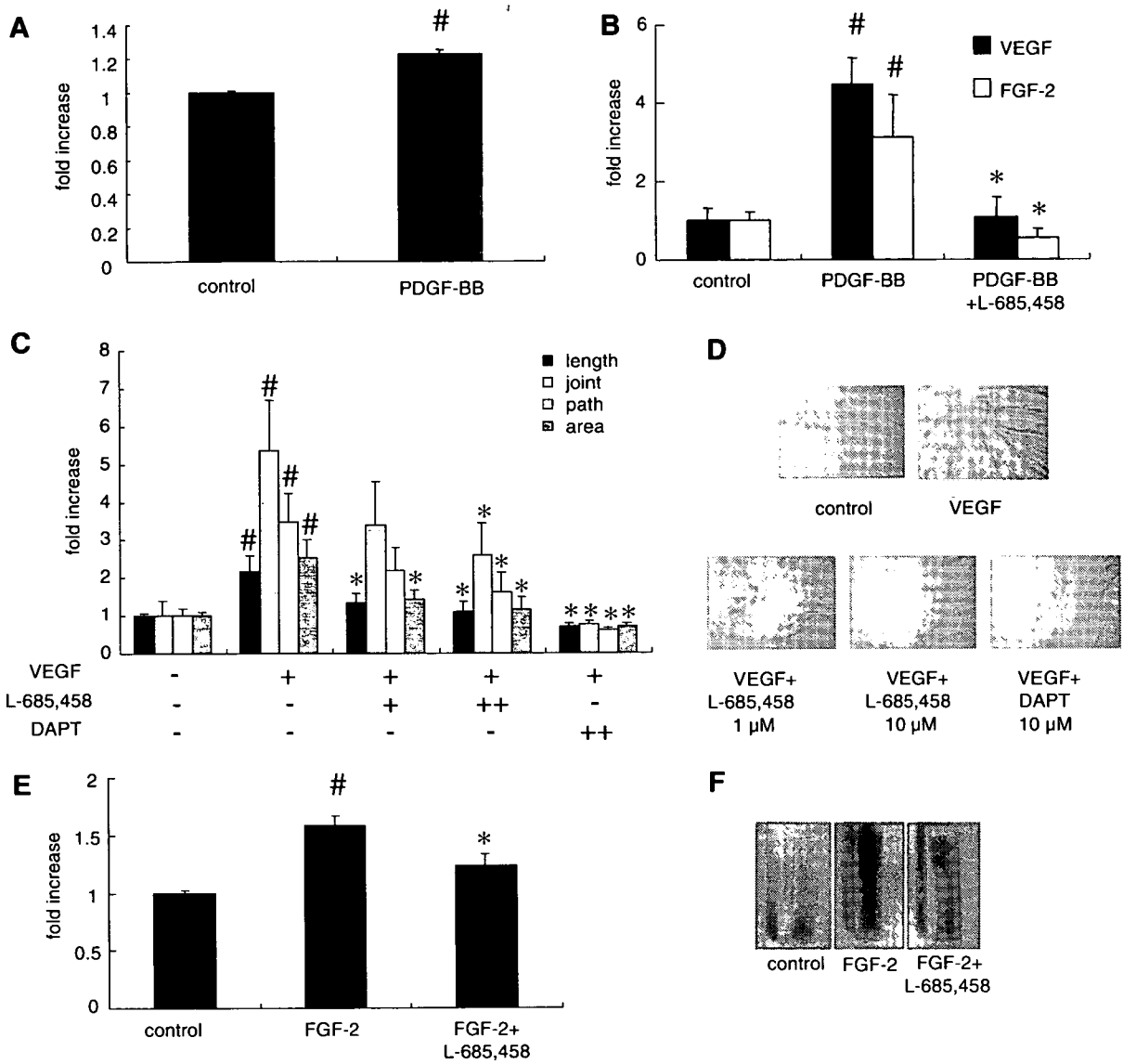

Fig. 4. The suppressive effect of L-685,458 on angiogenic growth factor production, tube formation, and angiogenesis in matrigel *in vivo*. (A) γ-Secretase activity of HASMC treated with or without PDGF-BB (10 ng/ml) for 24 h. "control" indicates no treatment. $^{\#}p < 0.001$ vs. control. (B) The mRNA levels of VEGF and FGF-2 in HASMC were quantified by real-time-qPCR. "control" indicates no treatment (DMSO). "PDGF-BB" indicates treatment with hrPDGF-BB 10 ng/ml. "L-685,458" indicates treatment with L-685,458 5 μM. $^{\#}p < 0.05$ vs. control, $^{*}p < 0.05$ vs. PDGF-BB. (C) Tube length, joint, path, and area were quantified by scoring software. HAEC treated with GSI (L-685,458 + = 1 μM ++ = 10 μM, DAPT ++ = 10 μM) in the presence of hrVEGF 10 ng/ml for 24 h. $^{\#}p < 0.05$ vs. no treatment, $^{*}p < 0.05$ vs. treatment with VEGF. (D) Representative pictures of tube formation (40× magnification). "control" indicates no treatment (DMSO). "VEGF" indicates treatment with hrVEGF 10 ng/ml. "L-685,458, 1 or 10 μM" indicates treatment with L-685,458, 1 or 10 μM. "DAPT 10 μM" indicates treatment with DAPT 10 μM. (E) Quantification of fluorescence of FITC-conjugated lectin-stained EC that had migrated into angioreactors. "control" indicates no treatment (DMSO). "FGF-2" indicates treatment with rFGF-2 250 ng/ml, "L-685,458" indicates treatment with L-685,458 20 μM. $^{\#}p < 0.01$ vs. control. $^{*}p < 0.05$ vs. FGF-2. (F) Representative pictures of matrigel using angioreactors. "control" indicates no treatment (DMSO). "FGF-2" indicates treatment with rFGF-2 250 ng/ml. "L-685,458" indicates treatment with L-685,458 20 μM.

increased secretion of Aβ, indicative of an increase in γ-secretase activity [27]. The present data showed that the activation of γ-secretase increased EC growth. γ-Secretase would be activated by VEGF and hypoxia, and regulate a part of VEGF function in the downstream signaling. Interestingly, our results suggest that γ-secretase can regulate the expression of VEGF, which suggests the auto-regulatory loop between VEGF and γ-secretase. We speculate that this dual regulatory system of γ-secretase in EC and SMC might be important to amplify and sustain the angiogenic action.

Thus, in combination with data from previous reports, observations from the present study suggest that γ-secretase regulates postnatal angiogenesis and that γ-secretase may be a useful therapeutic target for the modulation of angiogenesis in adults.

Disclosure

None.

Acknowledgments

We thank Prof. Michael T. Chin of Washington University and Prof. Maemura of Tokyo University for providing the VEGF-promoter plasmid. pCS2 + Notch1 ICV 6mt (Notch1 intracellular domain-6-myc-tagged) and pCS2 + Notch1 ΔE_{TM} 6mt (Notch1 extracellular transmembrane domain-6myc-tagged) were kindly gifted from Dr. Kopan (Washington University, St. Louis, MO).

Appendix A. Supplementary data

Supplementary data associated with this article can be found, in the online version, at doi:10.1016/j.bbrc.2007.09.003.

References

[1] B. De Strooper, Aph-1, Pen-2, and Nicastrin with Presenilin generate an active gamma-Secretase complex, Neuron 38 (2003) 9–12.
[2] W.T. Kimberly, M.J. LaVoie, B.L. Ostaszewski, W. Ye, M.S. Wolfe, D.J. Selkoe, Gamma-secretase is a membrane protein complex comprised of presenilin, nicastrin, Aph-1, and Pen-2, Proc. Natl. Acad. Sci. USA 100 (2003) 6382–6387.
[3] G. Yu, M. Nishimura, S. Arawaka, D. Levitan, L. Zhang, A. Tandon, Y.Q. Song, E. Rogaeva, F. Chen, T. Kawarai, A. Supala, L. Levesque, H. Yu, D.S. Yang, E. Holmes, P. Milman, Y. Liang, D.M. Zhang, D.H. Xu, C. Sato, E. Rogaev, M. Smith, C. Janus, Y. Zhang, R. Aebersold, L.S. Farrer, S. Sorbi, A. Bruni, P. Fraser, P. St George-Hyslop, Nicastrin modulates presenilin-mediated notch/glp-1 signal transduction and betaAPP processing, Nature 407 (2000) 48–54.
[4] S.F. Lee, S. Shah, H. Li, C. Yu, W. Han, G. Yu, Mammalian APH-1 interacts with presenilin and nicastrin and is required for intramembrane proteolysis of amyloid-beta precursor protein and Notch, J. Biol. Chem. 277 (2002) 45013–45019.
[5] H. Steiner, E. Winkler, D. Edbauer, S. Prokop, G. Basset, A. Yamasaki, M. Kostka, C. Haass, PEN-2 is an integral component of the gamma-secretase complex required for coordinated expression of presenilin and nicastrin, J. Biol. Chem. 277 (2002) 39062–39065.
[6] M. Nakajima, S. Yuasa, M. Ueno, N. Takakura, H. Koseki, T. Shirasawa, Abnormal blood vessel development in mice lacking presenilin-1, Mech. Dev. 120 (2003) 657–667.
[7] L. Serneels, T. Dejaegere, K. Craessaerts, K. Horre, E. Jorissen, T. Tousseyn, S. Hebert, M. Coolen, G. Martens, A. Zwijsen, W. Annaert, D. Hartmann, B. De Strooper, Differential contribution of the three Aph1 genes to gamma-secretase activity in vivo, Proc. Natl. Acad. Sci. U S A 102 (2005) 1719–1724.
[8] I. Greenwald, LIN-12/Notch signaling: lessons from worms and flies, Genes Dev. 12 (1998) 1751–1762.
[9] S.S. Huppert, A. Le, E.H. Schroeter, J.S. Mumm, M.T. Saxena, L.A. Milner, R. Kopan, Embryonic lethality in mice homozygous for a processing-deficient allele of Notch1, Nature 405 (2000) 966–970.
[10] E. Boscolo, M. Folin, B. Nico, C. Grandi, D. Mangieri, V. Longo, R. Scienza, P. Zampieri, M.T. Conconi, P.P. Parnigotto, D. Ribatti, Beta amyloid angiogenic activity in vitro and in vivo, Int. J. Mol. Med. 19 (2007) 581–587.
[11] S. Cantara, S. Donnini, L. Morbidelli, A. Giachetti, R. Schulz, M. Memo, M. Ziche, Physiological levels of amyloid peptides stimulate the angiogenic response through FGF-2, FASEB J. 18 (2004) 1943–1945.
[12] Z.J. Liu, T. Shirakawa, Y. Li, A. Soma, M. Oka, G.P. Dotto, R.M. Fairman, O.C. Velazquez, M. Herlyn, Regulation of Notch1 and Dll4 by vascular endothelial growth factor in arterial endothelial cells: implications for modulating arteriogenesis and angiogenesis, Mol. Cell. Biol. 23 (2003) 14–25.
[13] T. Nishikawa, H. Nakagami, A. Matsuki, A. Maeda, C.Y. Yo, T. Harada, R. Morishita, K. Tamai, Y. Kaneda, Development of high-throughput functional screening of therapeutic genes, using a hemagglutinating virus of Japan envelope vector, Hum. Gene Ther. 17 (2006) 470–475.
[14] H. Nakagami, R. Morishita, K. Yamamoto, Y. Taniyama, M. Aoki, K. Matsumoto, T. Nakamura, Y. Kaneda, M. Horiuchi, T. Ogihara, Mitogenic and antiapoptotic actions of hepatocyte growth factor through ERK, STAT3, and AKT in endothelial cells, Hypertension 37 (2001) 581–586.
[15] H. Nakagami, T.X. Cui, M. Iwai, T. Shiuchi, Y. Takeda-Matsubara, L. Wu, M. Horiuchi, Tumor necrosis factor-alpha inhibits growth factor-mediated cell proliferation through SHP-1 activation in endothelial cells, Arterioscler. Thromb. Vasc. Biol. 22 (2002) 238–242.
[16] K. Nakagawa, J.H. Oak, T. Miyazawa, Angiogenic potency of Amadori-glycated phosphatidylethanolamine, Ann. N. Y. Acad. Sci. 1043 (2005) 413–416.
[17] S. Beckert, F. Farrahi, R.S. Aslam, H. Scheuenstuhl, A. Konigsrainer, M.Z. Hussain, T.K. Hunt, Lactate stimulates endothelial cell migration, Wound Rep. Regen. 14 (2006) 321–324.
[18] S.K. Kim, H.J. Park, H.S. Hong, E.J. Baik, M.W. Jung, I. Mook-Jung, ERK1/2 is an endogenous negative regulator of the gamma-secretase activity, FASEB J. 20 (2006) 157–159.
[19] L. Guedez, A.M. Rivera, R. Salloum, M.L. Miller, J.J. Diegmueller, P.M. Bungay, W.G. Stetler-Stevenson, Quantitative assessment of angiogenic responses by the directed in vivo angiogenesis assay, Am. J. Pathol. 162 (2003) 1431–1439.
[20] N. Gupta-Rossi, E. Six, O. LeBail, F. Logeat, P. Chastagner, A. Olry, A. Israel, C. Brou, Monoubiquitination and endocytosis direct gamma-secretase cleavage of activated Notch receptor, J. Cell Biol. 166 (2004) 73–83.
[21] A. Fischer, N. Schumacher, M. Maier, M. Sendtner, M. Gessler, The Notch target genes Hey1 and Hey2 are required for embryonic vascular development, Genes Dev. 18 (2004) 901–911.
[22] C.K. Williams, J.L. Li, M. Murga, A.L. Harris, G. Tosato, Up-regulation of the Notch ligand Delta-like 4 inhibits VEGF-induced endothelial cell function, Blood 107 (2006) 931–939.
[23] M. Gessler, K.P. Knobeloch, A. Helisch, K. Amann, N. Schumacher, E. Rohde, A. Fischer, C. Leimeister, Mouse gridlock: no aortic coarctation or deficiency, but fatal cardiac defects in Hey2−/− mice, Curr. Biol. 12 (2002) 1601–1604.
[24] K. Takeshita, M. Satoh, M. Ii, M. Silver, F.P. Limbourg, Y. Mukai, Y. Rikitake, F. Radtke, T. Gridley, D.W. Losordo, J.K. Liao, Critical role of endothelial Notch1 signaling in postnatal angiogenesis, Circ. Res. 100 (2007) 70–78.
[25] A. Herreman, D. Hartmann, W. Annaert, P. Saftig, K. Craessaerts, L. Serneels, L. Umans, V. Schrijvers, F. Checler, H. Vanderstichele, V. Baekelandt, R. Dressel, P. Cupers, D. Huylebroeck, A. Zwijsen, F. Van Leuven, B. De Strooper, Presenilin 2 deficiency causes a mild pulmonary phenotype and no changes in amyloid precursor protein processing but enhances the embryonic lethal phenotype of presenilin 1 deficiency, Proc. Natl. Acad. Sci. USA 96 (1999) 11872–11877.
[26] J. Shen, R.T. Bronson, D.F. Chen, W. Xia, D.J. Selkoe, S. Tonegawa, Skeletal and CNS defects in Presenilin-1-deficient mice, Cell 89 (1997) 629–639.
[27] R. Wang, Y.W. Zhang, X. Zhang, R. Liu, X. Zhang, S. Hong, K. Xia, J. Xia, Z. Zhang, H. Xu, Transcriptional regulation of APH-1A and increased gamma-secretase cleavage of APP and Notch by HIF-1 and hypoxia, FASEB J. 20 (2006) 1275–1277.

Comparative roles of Twist-1 and Id1 in transcriptional regulation by BMP signaling

Masanori Hayashi[1,2], Keisuke Nimura[1], Katsunobu Kashiwagi[1], Taku Harada[1], Kunio Takaoka[3], Hiroyuki Kato[2], Katsuto Tamai[1] and Yasufumi Kaneda[1,*]

[1]Division of Gene Therapy Science, Graduate School of Medicine, Osaka University 2-2 Yamada-oka, Suita, Osaka 565-0871, Japan
[2]Department of Orthopedic Surgery, Shinshu University, 3-1-1 Asahi, Matsumoto, Nagano 390-8621, Japan
[3]Department of Orthopedic Surgery, Osaka City University Medical School, 1-4-3 Asahimachi, Abeno-ku, Osaka 545-8585, Japan
*Author for correspondence (e-mail: kaneday@gts.med.osaka-u.ac.jp)

Accepted 12 February 2007
Journal of Cell Science 120, 1350-1357 Published by The Company of Biologists 2007
doi:10.1242/jcs.000067

Summary

Basic helix-loop-helix (bHLH) transcription factors are known as key regulators for mesenchymal differentiation. The present study showed that overexpression of Twist-1, a bHLH transcription factor, suppresses bone morphogenetic protein (BMP)-induced osteoblast differentiation, and downregulation of endogenous Twist-1 enhances BMP signaling. Maximal inhibition of BMP signaling was observed when Twist-1 was bound to E47, which markedly enhanced the stability of Twist-1. Co-immunoprecipitation assays revealed that Twist-1 formed a complex with Smad4 and histone deacetylase (HDAC) 1 in MC3T3-E1 cells stably expressing Twist-1. With trichostatin, an HDAC inhibitor, osteogenic factors such as alkaline phosphatase, Runx2 and osteopontin increased. Those results suggested that Twist-1 inhibited BMP signaling by recruiting HDAC1 to Smad4.

Furthermore, the inhibitory effects of Twist-1 on BMP signaling were overcome by Id1 through induction of Twist-1 degradation. These findings suggest that Twist-1 can act as an inhibitor of BMP signaling, and Id1 can regulate BMP signaling through a positive feedback loop repressing Twist-1 function. These two molecules may therefore regulate differentiation of mesenchymal cells into progeny such as osteoblasts by controlling BMP signaling.

Key words: Twist-1, Id1, BMP, Smad, HDAC

Introduction

Members of the transforming growth factor (TGF)-β superfamily regulate important biological and developmental processes, including cell proliferation, differentiation and migration (Derynck and Zhang, 2003). This is achieved through the ability to induce or repress transcription of diverse gene targets. For example, differentiation of mesenchymal cells into components of bone, cartilage or adipose tissue is regulated by bone morphogenetic proteins (BMPs), which belong to the TGF-β superfamily. BMPs induce not only new bone formation in vivo when implanted into ectopic sites (Urist, 1965), but also osteoblast differentiation of mesenchymal cells in vitro (Katagiri et al., 1994; Thies et al., 1992). TGF-β/BMP signaling is initially mediated by interactions with heterodimeric complexes of type I and type II serine/threonine kinase receptors. Activated receptor kinases phosphorylate receptor-regulated Smads (R-Smads). R-Smads then form activated complexes with common-mediator Smads (C-Smads). These complexes translocate into the nucleus to act as transcriptional regulators (Derynck and Zhang, 2003; Massague, 2000; Wrana, 2000). Studies on the mechanisms by which Smads mediate TGF-β/BMP-regulated gene transcription have led to the discovery of co-activators and co-repressors (Derynck and Zhang, 2003). However, the molecular mechanisms underlying the inhibition of BMP signaling have not been fully elucidated.

Twist-1, originally identified in *Drosophila*, is a member of the basic helix-loop-helix (bHLH) family of proteins (Leptin, 1991; Thisse et al., 1987). Twist-1 is expressed in mesodermal and cranial neural crest cells during embryogenesis (Wolf et al., 1991). In homozygous Twist-1-knockout mice the cranial neural tube fails to close and they die at embryonic day 11.5 (Chen and Behringer, 1995). Twist-1 heterozygous mice present a craniosynostotic phenotype (Bourgeois et al., 1998). Expression of Twist-1 has been implicated in the inhibition of differentiation for multiple mesenchymal cell lineages, including muscle (Hebrok et al., 1997; Spicer et al., 1996) and bone cells (Lee et al., 1999; Rice et al., 2000). The mechanisms of inhibition have been well established in muscle (Hamamori et al., 1999; Hebrok et al., 1997; Spicer et al., 1996), but little is known about the mechanisms behind inhibition of osteoblast differentiation by Twist-1. Very recently, Twist-1 has been reported to interact directly with Runx2, a key transcriptional factor regulating osteogenic gene expression. Direct interaction of Twist-1 with Runx2 causes inhibited DNA binding of Runx2 followed by gene inactivation in osteoblast precursors (Bialek et al., 2004). The fact that neurogenin, another bHLH family member, inhibits glial cell differentiation by sequestering Smad1 of the transcription complex away from glial differentiation genes (Sun et al., 2001), suggests that Twist-1 may likewise affect BMP signaling in the process of mesenchymal cell differentiation into osteoblasts.

The best-studied example of dimerization partners for known tissue-specific bHLH transcription factors involves the gene products of the *E2A* gene (Lassar et al., 1991). Through differential splicing, this gene gives rise to two different bHLH

proteins, E12 and E47, the so-called E-proteins (Murre et al., 1989; Sun and Baltimore, 1991). Id is an internal dominant negative form of HLH transcription factor, lacking a basic region. By sequestering E-proteins, Id prevents myogenic transcription factors, such as MyoD, from forming heterodimer complexes (Benezra et al., 1990; Sun et al., 1991). Recent reports have indicated that BMP induces expression of Id1, resulting in degradation of tissue-specific bHLH transcription factors (Vinals et al., 2004; Vinals and Ventura, 2004). Furthermore, Id1 is critical to BMP-induced osteoblast differentiation (Peng et al., 2004). As a result, we hypothesized that Id1 may be an antagonist of Twist-1 in osteoblast differentiation. The present study found that Twist-1 inhibits BMP-induced osteoblast differentiation. Inhibition of BMP signaling by Twist-1 is enhanced by E-protein. Moreover, the inhibitory effect of Twist-1 is overcome by Id1 through the induction of Twist-1 degradation. These findings suggest that Twist-1 and Id1 can regulate differentiation of mesenchymal cell lineages by controlling BMP signaling.

Results

Overexpression of Twist-1 inhibits BMP-induced osteoblast-specific gene expression

To examine the effect of Twist-1 on expression of BMP2-induced osteoblast differentiation marker genes, a cell line (MC3T3-E1-Tw) stably expressing Twist-1 was established. Since MC3T3-E1 cells contained less endogenous Twist-1 (Tamura and Noda, 1999) and Id1 (data not shown) than C3H10T1/2 cells, the cell line was appropriate to minimize the effect of endogenous Twist-1 and Id1. Exogenous Flag-Twist-1 was detected in MC3T3-E1-Tw1 by western blotting of immunoprecipitates using anti-Flag antibody (Fig. 1A).

Next, ALP activity stimulated by BMP2 was examined. BMP2-induced ALP activity was elevated in parental cells (MC3T3-E1-WT; Fig. 1B). By contrast, Twist-1 overexpression significantly suppressed BMP2-enhanced ALP activity. Basal levels of ALP activity in untreated MC3T3-E1-WT and MC3T3-E1-Tw clone 1 (MC3T3-E1-Tw1) cells were low. We analyzed ALP activity under BMP stimulation in other stable transformant clones. ALP activity in all the clones (data not shown) was much lower than in the parental MC3T3-E1-WT. We further examined whether Twist-1 overexpression also suppressed expression of other osteoblast marker genes, such as osteopontin (Hullinger et al., 2001; Shi et al., 1999; Yang et al., 2000) and osteocalcin (Katagiri et al., 1994; Thies et al., 1992). The level of BMP2-induced osteopontin expression in MC3T3-E1-Tw1 cells was lower than in MC3T3-E1-WT cells. BMP2-induced osteocalcin expression also decreased in MC3T3-E1-Tw1 cells (Fig. 1C). These results indicate that Twist-1 could affect BMP2-induced osteoblast differentiation.

Downregulation of endogenous Twist-1 enhances transcriptional activity mediated by BMP signaling

To examine the function of Twist-1 in BMP signaling, we attempted to downregulate endogenous Twist-1 expression in C3H10T1/2, a mesenchymal progenitor cell line with high levels of Twist-1 expression, using RNA interference (RNAi) technology. We selected the most effective Twist-1-specific siRNA (siTwist-691). Transient transfection of siTwist-691 resulted in a 50-60% decreases in mRNA levels (Fig. 2A). Next, we examined the direct effects of downregulating

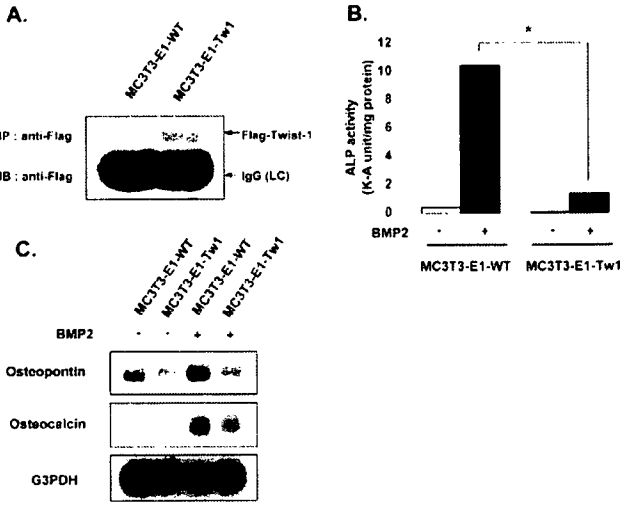

Fig. 1. Twist-1 overexpression suppresses BMP2-induced osteoblast differentiation. (A) Immunoprecipitation of overexpressed Flag-tagged Twist-1 in the nuclear extracts of MC3T3-E1-Tw1 and MC3T3-E1-WT cells. (B) MC3T3-E1-Tw1 and MC3T3-E1-WT cells were grown in the presence or absence of rhBMP2 (300 ng/ml) for 6 days. ALP activity was measured as described in the Materials and Methods (*P<0.01). (C) MC3T3-E1-Tw1 and MC3T3-E1-WT cells were grown in the presence or absence of rhBMP-2 (300 ng/ml) and total RNA was isolated on day 6. Northern blot analysis was performed using osteopontin and osteocalcin cDNA probes.

endogenous Twist-1 on transcriptional activity mediated by Smads using 3GC2-Lux, which contains three tandem repeats of a Smad-binding GC-rich sequence linked with the collagen X core promoter inserted into pGL2-Basic (Ishida et al., 2000). 24 hours after transfection of C3H10T1/2 cells with Twist-1-specific siRNA, cells were transfected with 3GC2-Lux and TK-*Renilla* luciferase and fed with or without rhBMP2 treatment. Suppression of endogenous Twist-1 expression by Twist-1-specific siRNA resulted in increased BMP-dependent Smad transcriptional activity (Fig. 2B). Additionally, when the siTwist-691 was co-transferred to C3H10T1/2 cells with Twist-1 expression plasmid by lipofection, real-time PCR analysis indicated that endogenous Twist-1 expression was partially recovered (at most 32% compared with Twist-1 level in the cells received the siRNA alone). However, no significant increase of endogenous Twist-1 expression was obtained using control plasmid, pCAGIP, without Twist-1 cDNA (data not shown).

Next, we overexpressed Smad1, Smad4 and BMPR-IB(QD) in C3H10T1/2. Downregulation of endogenous Twist-1 using Twist-1-specific siRNA also enhanced transcriptional activity mediated by overexpressed Smads (Fig. 2C). These results indicate that Twist-1 could inhibit BMP/Smad signaling.

Twist-1 inhibits BMP signaling cooperatively with E-protein

To examine whether overexpressed Twist-1 could inhibit BMP-induced transcriptional activity, co-transfection studies were performed. P19 cells that respond to BMPs and express some of the BMP target genes were transfected using Twist-1,

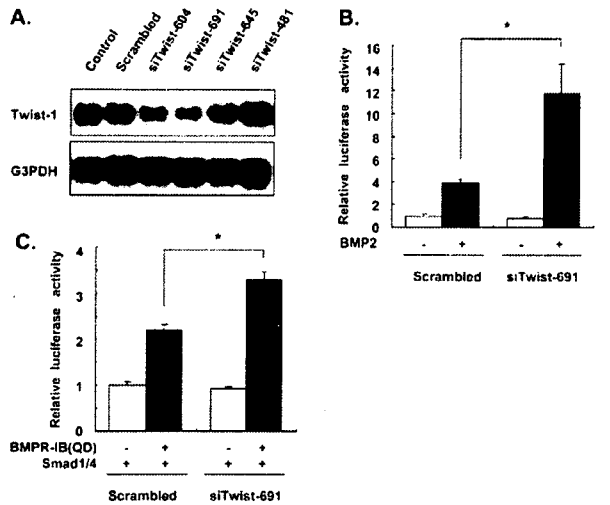

Fig. 2. Downregulation of endogenous Twist-1 using RNAi methods enhances BMP-induced transcriptional activity mediated by Smads. (A) C3H10T1/2 cells were transfected with either Twist-1-specific siRNA (siTwist-604, siTwist-691, siTwist-645, siTwist-481) or control siRNA (Scrambled) as described in the Materials and Methods. Total RNA was extracted 24 hours later, and northern blot analysis was performed using a Twist-1 cDNA probe. (B) C3H10T1/2 cells were transfected with either siTwist-691 or control siRNA (Scrambled). Cells were transfected with 3GC2-Lux and TK-*Renilla* luciferase 24 hours after siRNA transfection. At 12 hours after second transfection, cells were treated, with BMP (300 ng/ml) or left untreated, for 12 hours. Cells were lysed and luciferase activity was assayed (*P<0.01). The mean value of firefly luciferase and *Renilla* luciferase activity in the scrambled sample without BMP was approximately 2,000 and 34,000 RLU (relative light unit), respectively. (C) C3H10T1/2 cells were transiently transfected with either 90 pmol of siTwist-691 or Scrambled in combination with 100 ng of 3GC2-Lux luciferase construct, Smad1, Smad4 and BMPR-IB(QD). Cells were lysed and luciferase activity was assayed 24 hours after transfection (*P<0.01). The mean value of firefly luciferase and *Renilla* luciferase activity in the scrambled sample without BMPR-1B(QD) was approximately 411,000 and 30,000 RLU, respectively.

Smad1 and Smad4 expression constructs and 3GC2-Lux containing a Smad-binding sequence. Co-transfection of BMPR-IB(QD) with Smad1 and Smad4 enhanced transcription of 3GC2-Lux (Fig. 3A). Exogenous Twist-1 inhibited this activity, but inhibitory effects were very weak. Since Twist-1 reportedly inhibits MyoD trans-activation by E-protein sequestration, and the Twist-1-E-protein heterodimer inhibits myocyte enhancer-binding factor 2 (MEF2) trans-activation by direct interaction (Spicer et al., 1996), we hypothesized that the Twist-1-E-protein heterodimer could also act as a repressor in BMP signaling. We examined the effects of E47, an alternatively spliced product of the *E2A* gene (Murre et al., 1989; Sun and Baltimore, 1991), on suppression of Smad signaling by Twist-1. Twist-1 bound to E47 further increased the inhibition of BMP-induced transcription of 3GC2-Lux in a dose-dependent manner (Fig. 3A).

Next, the effect of Twist-1 and E47 on TGF-β signaling was analyzed using 3TP-Lux, which was empirically designed to have maximal responsiveness to TGF-β (Wrana et al., 1992). However, TGF-β signaling was not inhibited by Twist-1 and E47. Id proteins are dominant-negative-type HLH proteins that lack the basic DNA-binding domain. In muscle development, Id1 forms heterodimers with E-protein and prevents myogenic bHLH proteins from forming complexes with E-protein (Benezra et al., 1990; Sun et al., 1991). BMP stimulation also reportedly induces Id1 expression (Katagiri et al., 1994; Nakashima et al., 2001; Ogata et al., 1993), an adverse pattern as compared to Twist-1 expression (Tamura and Noda, 1999). We therefore investigated whether Id1 also cooperated with E-protein to inhibit BMP signaling. In contrast to Twist-1, however, Id1 failed to repress BMP signaling in the presence or absence of E47 (Fig. 3B), suggesting distinctly different roles for Id1 and E47 in BMP signaling. Moreover E47 also failed to repress Smad signaling without Twist-1 (Fig. 3B). To assess whether formation of heterodimer complex with E-protein is critical for the inhibitory effect of Twist-1, we overexpressed a Twist-1 mutant (Twist-NBCT), which lacks the HLH domain (El Ghouzzi et al., 2000; Hamamori et al., 1997; Hebrok et al., 1997; Spicer et al., 1996). This Twist-1 mutant did not interact with E-protein (Fig. 3C). In contrast to with wild-type Twist-1, Twist-NBCT failed to suppress transcriptional activity in the presence or absence of E47 (Fig. 3D). These findings suggest that maximal inhibition of BMP signaling by Twist-1 requires heterodimer formation with E-protein. Additionally, by over expression of Twist-1 and E47, the inhibition of luciferase gene expression by siRNA was abolished (Fig. 3E).

Twist-1 inhibited BMP signaling by recruiting HDAC1 to the Smad1-Smad4 complex

Histone deacetylases (HDACs) are involved in the repression of MyoD and MEF2 by Twist-2, which shares high homology with Twist-1 (Gong and Li, 2002; Li et al., 1995; Tamura and Noda, 1999). To analyze the involvement of HDAC in the inhibition of BMP signaling by Twist-1, Flag-tagged Twist-1 was immunoprecipitated using anti-Flag antibody in MC3T3-E1-Tw1 and the presence of HDAC and Smad was investigated in the precipitate. As shown in Fig. 4A, HDAC1 and Smad4 were detected in the precipitate, but not Smad1. In MC3T3-E1-WT, neither HDAC1 nor Smad4 was precipitated. Next, trichostatin (TSA), an HDAC inhibitor, was used to rescue the inhibition of osteogenic gene expression mediated by Twist-1. As shown in Fig. 4B, TSA treatment significantly increased the expression of ALP, Runx2 and osteopontin in the MC3T3-E1-Tw1 under BMP2 stimulation. These results suggested that Twist-1could inhibit BMP signaling by recruiting HDAC1 to Smad complex via Smad4.

Twist-1 protein stability is increased by the formation of heterodimer complex with E-protein

Stability of bHLH proteins is reportedly increased by the formation of heterodimer complexes with other bHLH proteins (Deed et al., 1996; Vinals et al., 2004; Vinals and Ventura, 2004). We therefore examined whether co-expression of E47 increases the level of Twist-1 protein. Myc-tagged Twist-1 was expressed with or without Myc-tagged E47 in COS-7 cells, and the levels of both were immunodetected by western blotting. Co-expression of E47 greatly increased Twist-1 protein levels (Fig. 5A). Next, to determine whether enhancement of Twist-1 protein expression is caused by

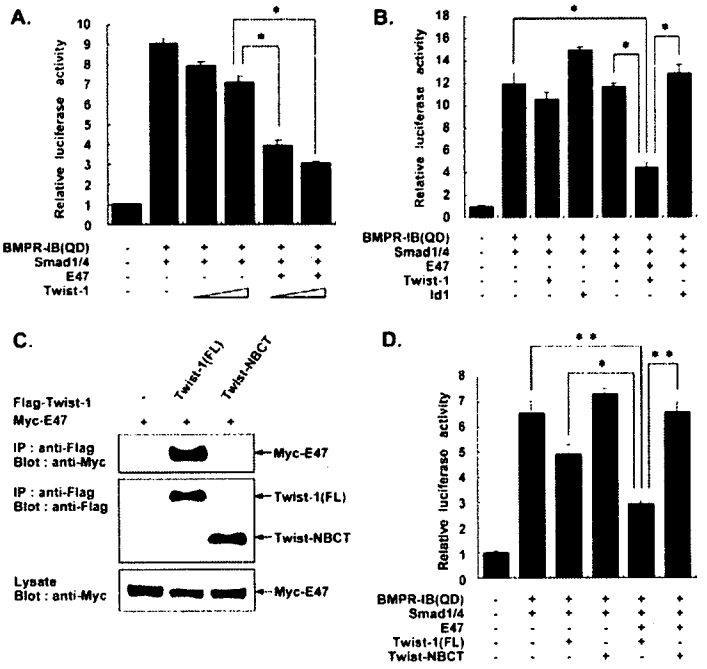

Fig. 3. Twist-1 inhibits BMP-induced Smad transcriptional activity with E-protein. (A) P19 cells were transiently transfected with 3GC2-Lux luciferase construct in combination with 50 ng of BMPR-IB(QD), Smad1, Smad4, E47 and increasing doses (12.5 or 50 ng) of Twist-1 expression construct. Cells were lysed and luciferase activity was assayed 24 hours after transfection (*P<0.01). The mean value of firefly luciferase and *Renilla* luciferase activity in cells transfected with luciferase expression plasmids was approximately 109,000 and 681,000 RLU, respectively. (B) P19 cells were transiently transfected with 3GC2-Lux luciferase construct in combination with 50 ng of BMPR-IB(QD), Smad1, Smad4, E47, Twist-1 and Id1 construct. Cells were lysed and luciferase activity was assayed 24 hours after transfection (*P<0.01). The mean value of firefly luciferase and *Renilla* luciferase activity in cells transfected with luciferase expression plasmids was approximately 51,000 and 199,000 RLU, respectively. (C) Flag-tagged full-length (FL) Twist-1 or deletion Twist-1 mutant (Twist-NBCT) and Myc-tagged E47 constructs were transfected into COS-7 cells. Lysates were immunoprecipitated using anti-Flag antibody and blotted with anti-Myc antibody. (D) P19 cells were transiently transfected with 3GC2-Lux luciferase construct in combination with 50 ng of BMPR-IB(QD), Smad1 and Smad4, E47, full-length Twist-1 and deletion Twist-1 mutant (Twist-NBCT) expression construct. Cells were lysed and luciferase activity was assayed 24 hours after transfection (**P<0.01, *P<0.05).

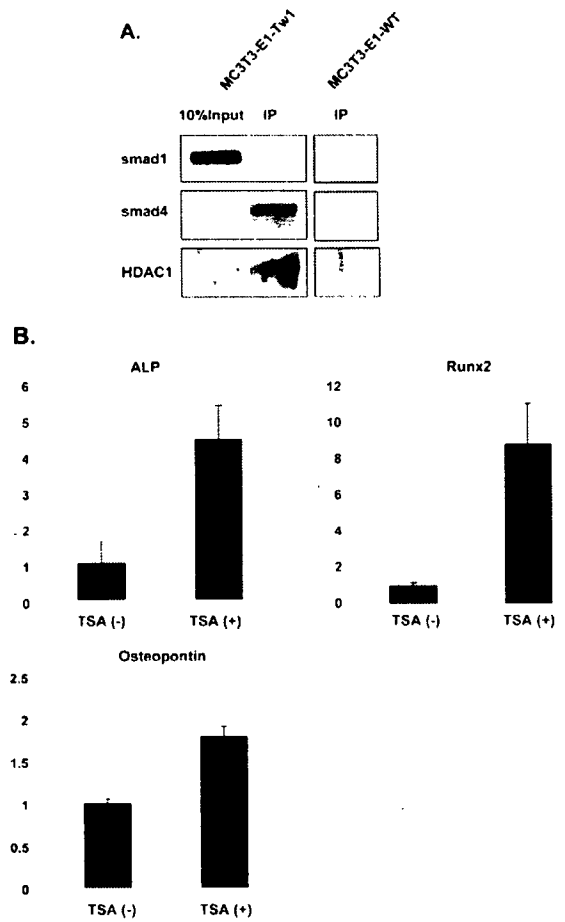

avoidance of degradation, we examined Twist-1 protein turnover using a pulse-chase assay. Twist-1 was rapidly degraded in cells, with protein levels at 180 minutes reduced to 17% compared with the baseline at 0 minutes. By contrast, Twist-1 protein stability was greatly enhanced by co-expression with E47 (Fig. 5B). Recent reports have shown that Id genes are rapidly upregulated by BMP stimulation (Nakashima et al., 2001; Ogata et al., 1993; Peng et al., 2004). BMP2 decreases myogenin and Mash1 protein stability through induction of Id1 (Vinals et al., 2004; Vinals and Ventura, 2004). In addition, our previous data showed that Twist-1 could inhibit BMP signaling (Fig. 3A,B,D). These results prompted us to investigate whether Id1 would induce Twist-1 degradation and inhibit Twist-1 function. Twist-1 was degraded by co-transfection of Id1 in the presence of E47 (Fig. 5B).

Id1 inhibits Twist-1 function by interfering with functional Twist-1-E47 heterodimer formation

The finding that Twist-1 stabilization by E47 was partially lost by co-transfection of Id1 suggests that Id1 may sequester E47 from Twist-1, resulting in Twist-1 degradation. We tested this

Fig. 4. Twist-1 can interact with HDAC1 and Smad4. (A) MC3T3-E1-WT and MC3T3-E1-Tw1 cells were treated with BMP2 (300 ng/ml) for 24 hours. Lysates were immunoprecipitated using anti-Flag antibody and blotted with anti-Smad4 and HDAC1 antibody. 10% In, 10% of input; IP, immunoprecipitated fraction. (B) MC3T3-E1-Tw1 cells were treated with BMP alone [TSA (–)] or the mixture of BMP and TSA (82.5 μM) [TSA (+)]. After 24 hours, total RNA was extracted and the expression of ALP, Runx2 and osteopontin was quantified by real-time PCR. The expression levels were normalized by GAPDH, and the ratio was shown in each sample. Data are presented as mean ± s.d. of triplicate samples (*P<0.05).

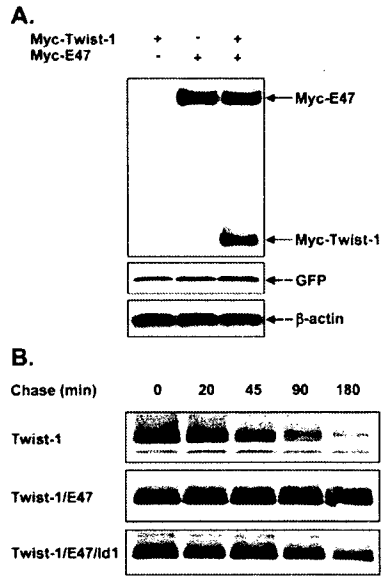

Fig. 5. Twist-1 protein stability is increased by the formation of a heterodimer complex with E47. (A) Myc-tagged Twist-1 and E47 constructs and GFP expression vector were transfected into COS-7 cells. Western blot analysis was performed with anti-Myc antibody. To show transfection efficiency, GFP protein was also detected by western blot. (B) COS-7 cells were transfected with the Flag-tagged Twist-1, Myc-tagged E47 and/or Myc-tagged Id1. At 24 hours after transfection, cells were pulsed with [^{35}S]methionine and cysteine for 3 hours, and chased with unlabeled medium for the indicated times. Labeled cell lysates were immunoprecipitated using anti-Flag antibody. Flag-tagged Twist-1 was visualized using SDS-PAGE.

possibility using immunoprecipitation assay in COS-7 cells. Increasing doses of Id1 decreased the amounts of E47 co-immunoprecipitated with Twist-1 (Fig. 6A). The amount of immunoprecipitated Twist-1 was also decreased by co-transfection of Id1, suggesting that Id1 induces Twist-1 degradation by sequestering E47 from Twist-1.

To examine whether Twist-1 also interferes with Id1-E47 heterodimer formation, we next performed the same experiment by replacing Id1 with Twist-1. In contrast to Id1, Twist-1 failed to interfere with Id1-E47 heterodimer formation (Fig. 6B). These results suggest that Id1 interacts with E47 more strongly than Twist-1 does, resulting in sequestration of E47 from Twist-1. In C3H10T1/2, endogenous Id1 was also co-immunoprecipitated with E47 using anti-E47 antibody (Fig. 6C). We examined the possibility that Id1 could rescue the inhibitory effect of Twist-1 on BMP signaling by inducing Twist-1 degradation. Twist-1-induced inhibition of BMP signaling was overcome by Id1 in a dose-dependent manner (Fig. 6D). It has been reported that differentiation of osteoblastic cells is promoted by transient expression of Id1 in early developmental stages (Peng et al., 2004). We attempted to rescue the inhibition of BMP signaling by Id1 gene transfer to MC3T3-E1-Tw1. As shown in Fig. 6E, the recovery of ALP activity in MC3T3-E1-Tw1 by Id1 gene transfer was significantly higher than by GFP gene transfer. These findings indicate that Id1 may regulate BMP signaling through a positive feedback loop that represses Twist-1 function.

Discussion

During embryonic mesoderm development, BMPs play critical roles in the commitment of mesenchymal cells into osteoblast and chondroblast lineages (Centrella et al., 1994; Hogan, 1996). Smads phosphorylated by BMP stimulation translocate into the nucleus and interact in transcription complexes with several DNA-binding transcription factors or cofactors that affect gene activation (Derynck and Zhang, 2003; Massague, 2000; Wrana, 2000). These factors have been considered critical for a variety of responses to BMP signaling in different BMP-targeted genes. Also, several inhibitors of BMP signaling have been reported. For example, Smad6 inhibits BMP/Smad1 signaling by acting as a selective Smad4 decoy (Hata et al., 1998). Tob, a member of the anti-proliferative protein family, binds Smad1, Smad5 and Smad8, and inhibits Smad-mediated transcriptional activities (Yoshida et al., 2000). Smads have also been shown to interact with bHLH transcription factors. For example, Smad3 directly interacts with MyoD and represses transcriptional activity (Liu et al., 2001). Neurogenin, another bHLH transcription factor, binds to both Smad1 and CBP (CREB-binding protein), and inhibits glial differentiation (Sun et al., 2001). The present study provides the first report that Twist-1, a DNA-binding bHLH transcription factor, inhibits transcriptional activities mediated by Smads (Fig. 3A,B,D).

Twist-1 reportedly acts as an inhibitor of muscle differentiation by sequestering E-protein from MyoD and blocking DNA binding, and by inhibiting trans-activation by MEF2 (Spicer et al., 1996). Twist-2 also requires heterodimerization with E-protein for inhibition of MyoD and MEF2 (Gong and Li, 2002), as seen with Twist-1. In addition, HDACs are involved in the repression of MyoD by Twist-1 and -2. In our results, Twist-1 also required heterodimerization with E47 for both maximal inhibition of Smad-mediated transcriptional activity (Fig. 3A,B,D) and increasing Twist-1 protein stability (Fig. 5B). BMPs activate transcription through physical interaction and functional cooperation of R-Smads and coactivators CBP and/or p300 (Derynck and Zhang, 2003). Our result (Fig. 4A,B) supports the possibility that the inhibition of BMP signaling by Twist-1 and E47 was mediated by direct recruitment of HDAC1 to Smad complexes via Smad4. The repression of HDAC by TSA increased the expression of osteogenic factors probably by the activation of BMP signaling. However, gel-shift assay of Smads revealed that Twist-1 failed in the inhibition of DNA binding of Smads (data not shown). This result was not contradictory to the involvement of HDAC in inhibitory mechanism by Twist-1.

We also showed that the effect of Twist-1 in repressing BMP signaling was abrogated by Id1 (Fig. 6D,E). Id1 expression is induced by BMP stimulation in mesenchymal and neuroepithelial cells (Katagiri et al., 1994; Nakashima et al., 2001; Ogata et al., 1993). Id1 lacks the basic region necessary for binding to the E-box and acts as a dominant negative regulator by sequestering E-protein (Benezra et al., 1990). Furthermore, Id1 sequesters E-proteins away from myogenin and inhibits myogenesis by accelerating myogenin degradation (Vinals and Ventura, 2004). In neural development, transient induction of Id1 by BMP2 decreases Mash1 stability and restricts neuronal differentiation by the same mechanism (Vinals et al., 2004). These findings support the possibility that Id1 may positively regulate BMP signaling

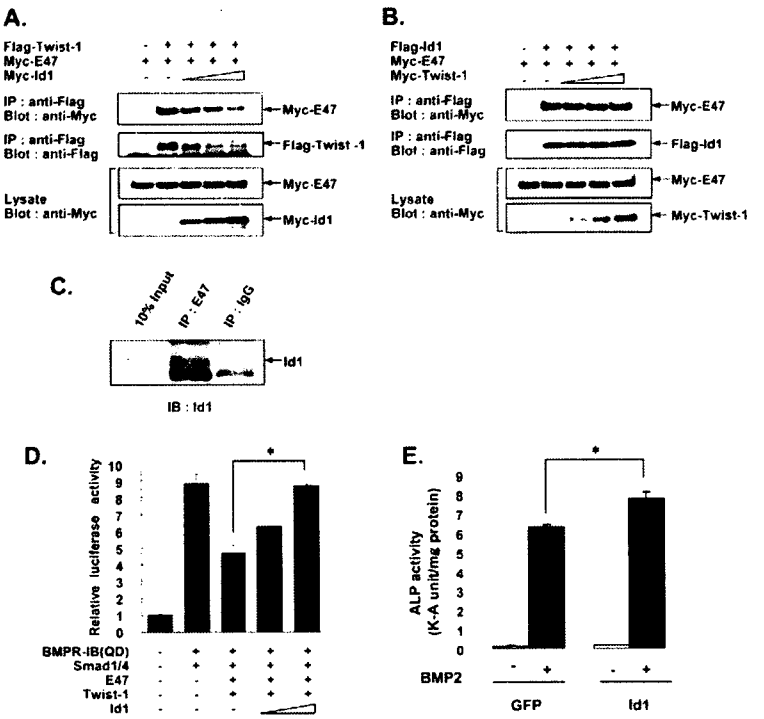

Fig. 6. Id1 inhibits Twist-1 function by sequestering E47 from Twist-1. (A) COS-7 cells were transiently transfected with Flag-Twist-1, Myc-tagged E47 and increasing doses (0.5, 1 or 2 μg) of Myc-tagged Id1 construct. Lysates were immunoprecipitated using anti-Flag antibody and blotted with anti-Flag and anti-Myc-antibody. (B) COS-7 cells were transiently transfected with Flag-Id1, Myc-tagged E47 and increasing doses (0.5, 1 or 2 μg) of Myc-tagged Twist-1 construct. Lysates were immunoprecipitated using anti-Flag antibody and blotted with anti-Flag and anti-Myc-antibody. (C) Endogenous E47 in C3H10T1/2 cells was precipitated using anti-E47 antibody. Then, Id1 was detected in the immunoprecipitates by western blot. (D) P19 cells were transiently transfected with 3GC2-Lux luciferase construct in combination with 50 ng of BMPR-IB(QD), Smad1 and Smad4, 25 ng of Twist-1 and E47, and increasing doses (25 or 100 ng) of Id1 expression construct. Cells were lysed and luciferase activity was assayed 24 hours after transfection (*P<0.01). (E) MC3T3-E1-Tw1 cells were transiently transfected with either Id1 or GFP expression construct by electroporation (Amaxa). The cells were grown in the presence or absence of rhBMP2 (300 ng/ml) for 6 days. ALP activity was measured as described in the Materials and Methods. Data are presented as mean ± s.d. of triplicate samples (*P<0.05).

by sequestering E-protein from Twist-1 to accelerate degradation. As shown in Fig. 6E, the recovery of ALP activity in MC3T3-E1-Tw1 by Id1 gene transfer was significantly higher than by GFP gene transfer, but the effect was not as much as expected from co-transfection experiment (Fig. 6D). We estimated that transient expression of Id1 was not sufficient to completely overcome the effect of stably expressing Twist-1, because transfection efficiency was not as high (at most 20%) in MC3T3-E1 cells.

In response to BMP stimulation, C3H10T1/2 embryonic mesenchymal cells express bone markers including collagen type I, ALP, osteopontin and osteocalcin (Ju et al., 2000). The osteopontin gene is reportedly a target of the BMP signaling pathway. Smad1 activates the osteopontin promoter by preventing Hoxc-8 (which negatively regulates osteopontin expression) from binding to this promoter (Shi et al., 1999; Yang et al., 2000). In addition, BMP stimulates direct binding of Smad proteins to the targeting sequence of the osteopontin promoter and activates transcription (Hullinger et al., 2001). In this study, we found that overexpression of Twist-1 repressed BMP2-induced expression of osteopontin and osteocalcin, and ALP activity (Fig. 1B,C). It is also known that Runx2 activates the expression of ALP, osteopontin and osteocalcin (Ducy et al., 1997; Harada et al., 1999). Furthermore, Twist-1 directly inhibits Runx2 (Bialek et al., 2004). From these reports, there is a possibility that the inhibition of BMP signaling in our experiments might result from an indirect effect mediated by the inhibition of Runx2. However, by direct binding with Runx2, Smads activate the transcription of Runx2 (Lee et al., 2000; Zhang et al., 2000). Moreover, BMP signaling was suppressed in co-transfection experiments using a reporter gene without the Runx2 recognition DNA sequence, as shown in Fig. 3A,B. Therefore, in addition to an indirect effect, through the inhibition of Runx2, it is likely that Twist-1 may have a direct inhibitory effect on BMP signaling.

We also showed that Smad-dependent transcriptional activity was enhanced by siRNA-mediated downregulation of endogenous Twist-1 in transient transfection analysis with a reporter construct containing BMP-responsive elements (Fig. 2B,C). Levels of Twist-1 expression gradually decrease during osteoblast differentiation (Bialek et al., 2004; Rice et al., 2000; Tamura and Noda, 1999). Taken together these results indicate that Twist-1 may maintain the population of undifferentiated mesenchymal cells by inhibiting BMP-induced osteoblast differentiation. Our data indicate a novel mechanism by which the cellular effects of BMP signals can be potentially regulated through direct competition between Twist-1 and Id1 for binding to E-protein.

Materials and Methods

Plasmid construction

Mouse Twist-1, E47, Id1 and Smad1 and Smad4 were amplified using polymerase chain reaction (PCR) from cDNA templates, which were reverse transcribed from mRNA of C3H10T1/2. To create mammalian expression vectors Myc-Twist-1, E47, Id1, Flag-Twist-1, Smad1 and Smad4, cDNA clones were introduced using Gateway technology (Invitrogen, San Diego, CA) into pCAGIP-Myc and pCAGIP-Flag vectors (Niwa et al., 2002). For Flag-Twist-1 deletion mutants, Twist-NBCT (deletion of amino acids 125-169) were created by PCR, then introduced into pCAGIP-Flag using Gateway technology. To generate mammalian expression vectors pCMV-Twist-1, pCMV-E47, pCMV-Id1 and pCMV-Smad1 and pCMV-Smad4, the corresponding cDNA clones were introduced with Gateway technology into pcDNA3.1 (Invitrogen), which was converted into the destination vector. A 3GC2-Lux luciferase construct, the constitutively active form of BMP type I receptor [BMPR-IB(QD)] (Imamura et al., 1997) and the constitutively active form of TGF-β type I receptor [TβR-I(TD)] (Wieser et al., 1995) were kindly donated by Kohei Miyazono (University of Tokyo).

Cell culture and stable transfection

The C3H10T1/2 murine mesenchymal progenitor cell line, MC3T3E-1 osteoblastic cell line and COS-7 African green monkey SV40-transformed kidney fibroblast